



HAL
open science

Organic facies variability and paleoenvironmental changes on the Moroccan Atlantic coast across the Cenomanian-Turonian Oceanic Anoxic Event (OAE2)

Carolina Fonseca, João Graciano Mendonça Filho, Carine Lézin, Luís V. Duarte

► To cite this version:

Carolina Fonseca, João Graciano Mendonça Filho, Carine Lézin, Luís V. Duarte. Organic facies variability and paleoenvironmental changes on the Moroccan Atlantic coast across the Cenomanian-Turonian Oceanic Anoxic Event (OAE2). *International Journal of Coal Geology*, 2020, 230, pp.103587 -. 10.1016/j.coal.2020.103587 . hal-03491606

HAL Id: hal-03491606

<https://hal.science/hal-03491606>

Submitted on 22 Sep 2022

HAL is a multi-disciplinary open access archive for the deposit and dissemination of scientific research documents, whether they are published or not. The documents may come from teaching and research institutions in France or abroad, or from public or private research centers.

L'archive ouverte pluridisciplinaire **HAL**, est destinée au dépôt et à la diffusion de documents scientifiques de niveau recherche, publiés ou non, émanant des établissements d'enseignement et de recherche français ou étrangers, des laboratoires publics ou privés.



Distributed under a Creative Commons Attribution - NonCommercial 4.0 International License

1 **Organic facies variability and paleoenvironmental changes on the**
2 **Moroccan Atlantic coast across the Cenomanian—Turonian Oceanic**
3 **Anoxic Event (OAE2)**

4 Carolina Fonseca^{a*}, João Graciano Mendonça Filho^b, Carine Lézin^a, Luís V. Duarte^c

5

6 ^a Géosciences Environnement Toulouse, Université de Toulouse, CNES, CNRS, IRD, UPS, 14
7 avenue Édouard Belin, F-31400 Toulouse, France.

8 ^b Laboratório de Palinofácies e Fácies Orgânica (LAFO), Departamento de Geologia, Instituto
9 de Geociências, Universidade Federal do Rio de Janeiro, Av. Athos da Silveira, 274, prédio do
10 CCMN, sala J1020, Campus Ilha do Fundão, Cidade Universitária, CEP 21.949-900, Rio de
11 Janeiro, RJ, Brazil.

12 ^c University of Coimbra, MARE - Marine and Environmental Sciences Centre, Faculty of
13 Sciences and Technology, Department of Earth Sciences, Rua Sílvio Lima, 3030-790 Coimbra,
14 Portugal.

15 *carolina.fonseca@get.omp.eu (corresponding author)

16

17 **Abstract**

18 The Cenomanian—Turonian boundary is marked by worldwide paleoenvironmental and
19 paleoceanographical changes that are associated with a perturbation of the global carbon
20 cycle and black shale deposition, called the Oceanic Anoxic Event 2 (OAE2). The
21 objective of this study is to precisely characterize the nature of the organic matter, its
22 variability, paleoenvironmental significance and the preservation conditions of two
23 areas located along the northwest African Shelf where large-scale organic carbon burial
24 contributed significantly to the global carbon burial associated with OAE2.

25 With these premises, an organic petrographic and geochemical approach to the
26 Cenomanian—Turonian record of the Moroccan Atlantic coast allowed the definition of
27 the variability of the organic facies and the paleoenvironmental characterization of the
28 upper Cenomanian—lower Turonian sediments of the Agadir section (Agadir Basin)
29 and of the lower Turonian record of the Amma Fatma section (Tarfaya Basin).

30 At Agadir, the marine microplankton dominated assemblages, with variable degree of
31 amorphization, allowed the characterization of a transgressive-regressive cycle during
32 the upper Cenomanian followed, during the lower Turonian, by a drowning event with
33 establishment of a deep platform environment (under reducing conditions, increase in
34 EFU, EFV, EFMo). The base of the succession (base of *W. archaeocretacea* biozone)

35 and the top of the upper Cenomanian are characterized by two sea-level lowstands, a
36 high energy oxic environment that culminate in emersion surfaces (high EFMn and low
37 organic matter preservation).

38 The organic facies in the lower Turonian of Amma Fatma is largely dominated by
39 bacterial material (probably derived from sulfur bacteria), indicating an outer shelf
40 setting, with some degree of restriction, under euxinic conditions (high EFMo) and high
41 primary productivity (high EFCu, EFNi, EFZn).

42 Differences in terms of the redox conditions between the two basins during the lower
43 Turonian were determined, with anoxia prevailing at Agadir, while euxinic conditions
44 are established at Tarfaya. These are explained by different oceanic circulation patterns,
45 with the mixing of Tethyan waters at Agadir. High primary productivity is recorded at
46 both locations, possibly promoted by the occurrence of upwelling currents. This study
47 further corroborates a delay in the anoxia in Agadir, that during the isotopic excursion
48 of OAE2 only reaches slight dysoxia (upper Cenomanian), and the maintenance of
49 reducing conditions in Tarfaya post-OAE2.

50

51 **Keywords:** Organic matter; Palynofacies; Paleoenvironment; Agadir Basin; Tarfaya
52 Basin; Oceanic Anoxic Event 2

53

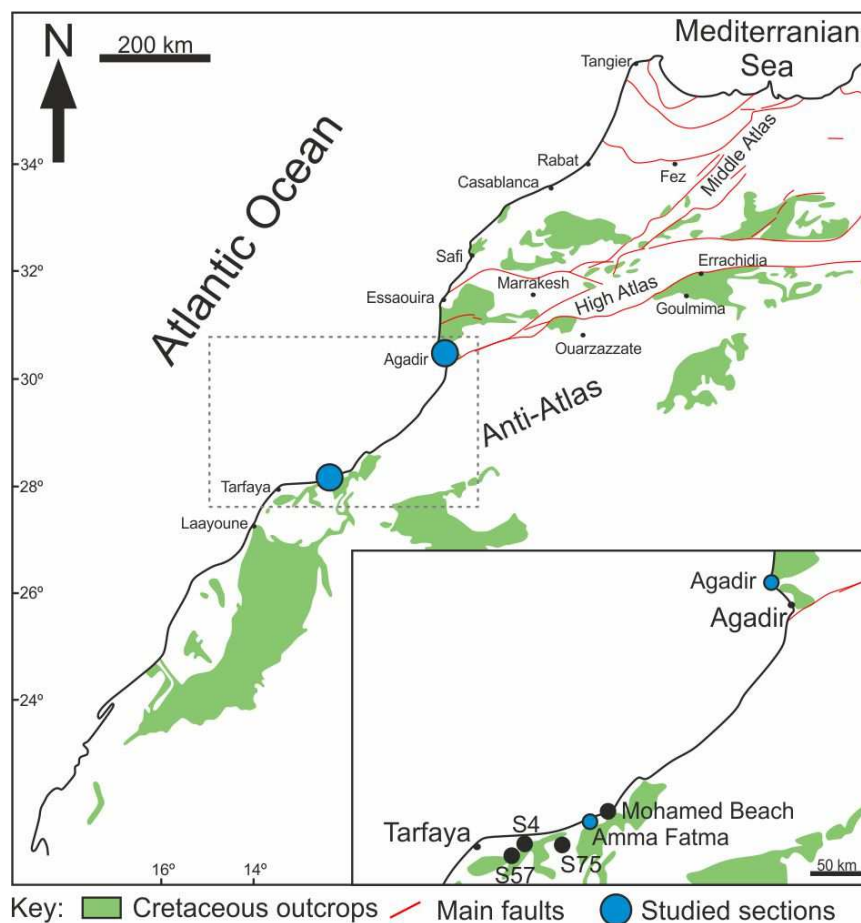
54 **1. Introduction**

55 High concentrations of greenhouse gases associated with increased tectonic activity and
56 the emplacement of large igneous provinces are thought to have promoted a very warm
57 climate and high sea-levels during mid to late Cretaceous (e.g. Larson, 1991; Sinton et
58 al., 1998; Larson and Erba, 1999; Wignall, 2001; Courtillot and Renne, 2003; Puc at et
59 al., 2003; Snow et al., 2005; Takashima et al., 2006; Forster et al., 2007; Turgeon and
60 Creaser, 2008; Sinninghe Damst  et al., 2010; Friedrich et al., 2012; O'Brien et al.,
61 2017; O'Connor et al., 2019). These conditions are linked to intermittent black shale
62 deposition in low-latitude basins of the North Atlantic and western Tethys, associated
63 with oceanic anoxic events (OAEs) (Jenkyns, 1980; Arthur et al., 1988; Kerr, 1998;
64 Leckie et al., 2002). The most geographically extensive event occurred during the latest
65 Cenomanian to early Turonian (OAE2) and is related to a major transgression, that
66 reached its peak during the early Turonian, and a warm climate (Huber et al., 1995,
67 2002; Clarke and Jenkyns, 1999; Norris et al., 2002; Voigt et al., 2004; Forster et al.,
68 2007; Haq, 2014). This event is characterized by a positive carbon isotope ($\delta^{13}\text{C}$)
69 excursion (CIE) and black shale deposition, with concomitant major faunal and floral
70 turnovers of the marine biota (Erbacher et al., 1996; Keller et al., 2001, 2008; Leckie et
71 al., 2002; Erba and Tremolada, 2004; Keller and Pardo, 2004; Hart and Leary, 1989;
72 Paul et al., 1999; Keller et al., 2001, 2004; Tsikos et al., 2004; Kuhnt et al., 2005;
73 Jenkyns, 2010; Lenniger et al., 2014; Owens et al., 2016).

74 Black shale deposition during OAE2 occurred worldwide in various paleogeographical
75 and paleobathymetric settings, from deep oceanic basins to shallow shelf seas
76 (Schlanger and Jenkyns, 1976; Jenkyns, 2010). This deposition was influenced by
77 several factors that controlled the degree of anoxia in the water column, such as,
78 primary productivity, terrestrial influx, sedimentation rates, organic matter (OM)
79 preservation, oxidation in the water column, water depth and distance to coast (Pedersen
80 and Calvert, 1990; Arthur and Sageman, 1994; Canfield, 1994). Inner ramp and coastal
81 environments are usually associated to sedimentary records with a deficit in black
82 shales, either by no deposition or no preservation (L ning et al., 2004).

83 The Moroccan Atlantic coast (Fig. 1) contains a diverse record of the OAE2, with
84 deeper shelf sections exhibiting organic-rich shale deposition prior, during and after the
85 CIE (e.g. Tarfaya Basin; Kuhnt et al., 1997, 2005, 2009; El Albani et al., 1999a,b;
86 Kolonic et al., 2002, 2005; L ning, 2004; Mort et al., 2007, 2008; Keller et al., 2008;
87 Gertsch et al., 2010; Trabucho Alexandre et al., 2010 and references therein), and

88 shallow neritic sections containing a sedimentary record extremely poor in OM during
 89 the CIE, with black shale deposition occurring only during the lower Turonian (e.g.
 90 Agadir Basin; Lüning et al., 2004; Gertsch et al., 2010; Jati et al., 2010; Fabre et al.,
 91 2018 and references therein). Several studies evoke high primary productivity,
 92 associated with upwelling, as the main mechanism controlling black shale deposition in
 93 the West African margin during the Late Cretaceous (Einsele and Wiedmann, 1982;
 94 Mort et al., 2008; Trabucho Alexandre et al., 2010; Fabre et al., 2018).
 95 This study examines the palynofacies and organic petrography of the upper
 96 Cenomanian—lower Turonian organic-rich record of the Moroccan Atlantic coast,
 97 namely from the reference sections of Agadir (Agadir Basin) and Amma Fatma
 98 (Tarfaya Basin), associated with isotope and elemental geochemical analyses with the
 99 aim of defining the organic facies variability in this shallow marine context, and to
 100 discuss the paleoenvironmental implications of the OAE2.
 101



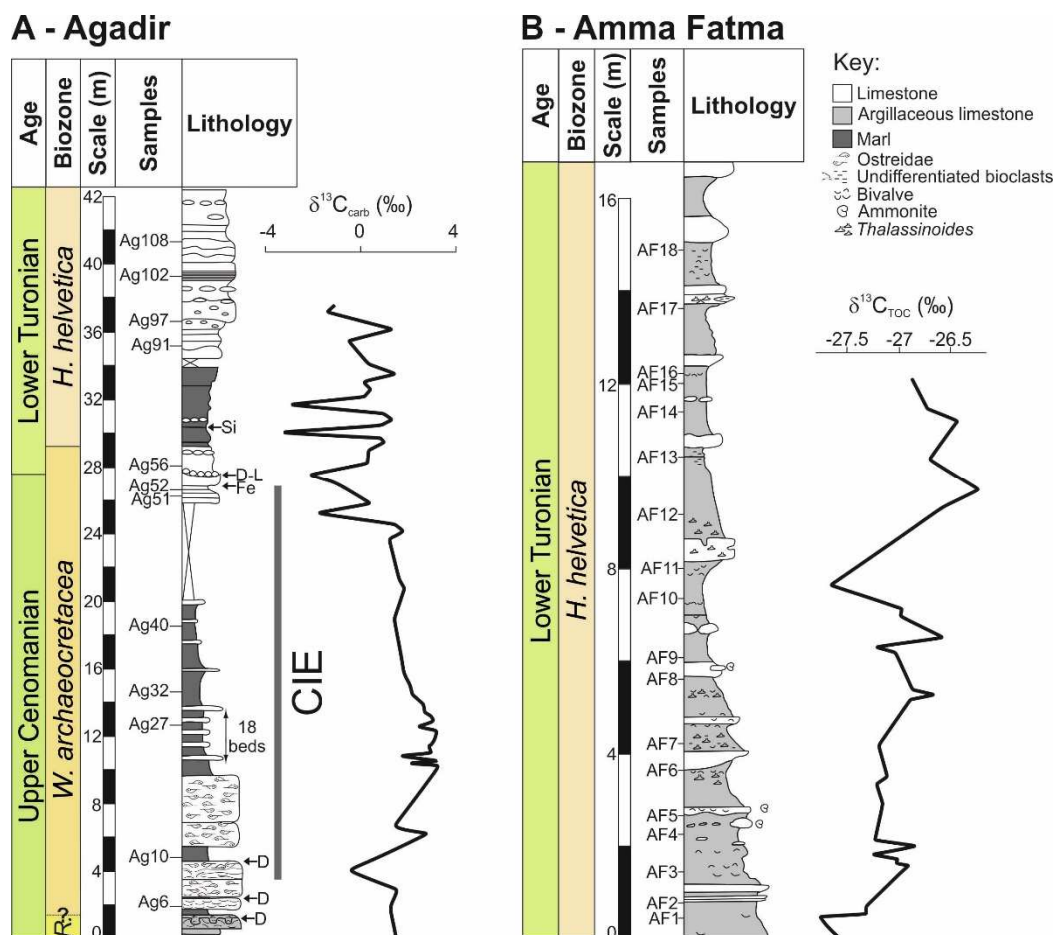
102
 103 Fig. 1. Simplified geological map of the Cretaceous outcrops in Morocco and location
 104 of the studied sections (adapted from Ettachfni and Andreu, 2004).
 105

106 **2. Geological Setting**

107 *2.1. Agadir Basin*

108 During the Cenomanian—Turonian, central Morocco was characterized by a large
109 marine seaway (“Atlas Gulf”) that represented a failed rift arm of the North Atlantic
110 Rift System (Lüning et al., 2004). This gulf was bordered by the Anti-Atlas to the South
111 and the Moroccan Meseta to the North, with the Agadir Basin representing, in part, the
112 western ending of the NE—SW trending High Atlas chain (Fig. 1). The Agadir section
113 is located along the coast, about 20 km North of the city of Agadir. Upper Cenomanian
114 (*Whiteinella archaeocretacea* biozone) sedimentation (~28 m) is characterized by
115 interbedded marl-limestone layers alternating with oyster-rich limestones, representing
116 a shallow subtidal to estuarine environment (Gertsch et al., 2010; Jati et al., 2010; Fig.
117 2, A). The lower Turonian (*W. archaeocretacea* and *Helvetoglobotruncana helvetica*
118 biozones, ~17m) is characterized by organic-rich limestones with chert and diagenetic
119 carbonate nodules, with the presence of low-oxygen-tolerant planktonic foraminifera,
120 suggesting a decrease in oxygen availability, possibly associated to an increase in
121 paleoproductivity (Fig. 2, A; Gertsch et al., 2010; Jati et al., 2010; Fabre et al., 2018).
122 Sea level interpretation was suggested by Gertsch et al. (2010) based on lithology,
123 macrofossils (oysters) and foraminiferal assemblages. Detailed 3rd order sea level cycles
124 were described by Lebedel (2013) based on lithological, sedimentological,
125 paleontological, and geochemical data. The positive $\delta^{13}\text{C}$ excursion related to the global
126 OAE2 event has been previously identified in the Agadir section by Gertsch et al.
127 (2010), and Jati et al. (2010).

128



129

130 Fig. 2. Stratigraphic logs of the studied sections with sample location. A: Agadir
 131 section; B: Amma Fatma section. Planktonic foraminifera biostratigraphy as defined by
 132 Smrzka et al. (2017) and Fabre et al. (2018), and carbon isotope excursion (CIE)
 133 interval as defined by Fabre et al. (2018). $\delta^{13}\text{C}_{\text{carb}}$ and $\delta^{13}\text{C}_{\text{TOC}}$ data from Jati et al.
 134 (2010) and Smrzka et al. (2017), respectively. R.: *Rotalipora cushmani* planktonic
 135 foraminifera biozone; D: Discontinuity; D-L: Discontinuity topped by lag deposits; Fe:
 136 Ferruginous level; Si: Chert.

137

138 2.2. Tarfaya Basin

139 The Tarfaya Basin is located along the coast of southern Morocco (NW Africa, 28°N—
 140 24°N) to the South of the Agadir Basin and the Anti-Atlas Mountains and extends into
 141 the Tindouf Basin to the East, the Senegal Basin to the South, and is bordered by the
 142 East Canary Ridge to the West (Fig. 1; Kolonic et al., 2002). This basin is one of several
 143 paleo-shelf basins located along the coasts of Senegal, Morocco and Tunisia, as part of
 144 the tectonically stable Sahara platform (El Albani et al., 1999a). According to El Albani
 145 et al. (1999a) and Kuhnt et al. (2001), it developed as a distal section of the proto-
 146 southern North Atlantic with water paleodepths between 200 to 300 m (outer shelf to
 147 upper bathyal waters). Since the late Cenomanian, this basin has undergone intense

148 upwelling, high primary production and the development of oxygen minimum
149 conditions. This lead to redox cycles on orbital time scales alternating between
150 sulphidic and anoxic ferruginous water column conditions (Kuhnt and Wiedmann,
151 1995; El Albani et al., 1999a, b; Kolonic et al., 2002, 2005; Poulton et al., 2015).

152 The Amma Fatma section is situated in the northern edge of the Tarfaya Basin (8km
153 SW of the Mohammed Plage) and consists of about 17 m of marly limestones
154 intercalated with carbonate concretions deposited during the aftermath of the OAE2,
155 representing an outer shelf context (Figs. 1 and 2, B; Smrzka et al., 2017). The presence
156 of discontinuous bioclastic storm beds with hummocky cross stratification is also
157 described (El Albani et al., 1999b). The marly sediments contain local *Thalassinoides*,
158 abundant peloids and no apparent macrofauna, with the exception of phosphatic fish
159 remains. Microfauna is represented by benthic and planktonic foraminifera (El Albani et
160 al., 1999a, 2001). The dark laminae of the marly sediments are mainly composed of clay
161 minerals and OM, while the lighter laminae display the presence of planktonic
162 foraminifera, some radiolarians, diatoms and pithonellids (El Albani et al., 2001). The
163 ammonite fauna and the planktonic foraminifera in the carbonate concretions date the
164 host sediment as early Turonian in age (*H. helvetica* biozone) (Smrzka et al., 2017).

165

166 **3. Materials and Methods**

167 A set of 30 samples was collected for analyses in this study. From the Agadir section 12
168 samples were selected: 7 from the upper Cenomanian and 5 from the lower Turonian
169 (Fig. 2, A). From the Amma Fatma section a group of 18 samples belonging to the
170 upper part of the lower Turonian were analyzed (Fig. 2, B). The samples studied in this
171 article were selected to highlight lithological, geochemical, and biological facies
172 variability described in previous works. The Agadir section samples are a subset of the
173 samples used by Fabre et al. (2018). The Amma Fatma section was sampled in the field,
174 in the same stratigraphic levels of the inorganic geochemical data published by Smrzka
175 et al. (2017).

176

177 *3.1. Palynofacies analysis*

178 Kerogen was isolated from the rock matrix at the Laboratory of Palynofacies and
179 Organic Facies of the Federal University of Rio de Janeiro (LAFO-UFRJ, Brazil)
180 following laboratory protocols for non-oxidative mineral-acid based palynology
181 processing (Tyson, 1995; Mendonça Filho et al. 2010b, 2014b). Between 20 to 40 g of

182 sediment was crushed (to about 2 mm in size) and carbonates, then silicates, and finally
183 any neoformed fluorides were removed by acid treatment (HCl 37% for 18 h, HF 40%
184 for 24 h, HCl 37% for 3 h, respectively). The kerogen was concentrated using ZnCl₂
185 (density=1.9 to 2 g/cm³) and a few drops of HCl (10%) is added to the organic fraction
186 (supernatant) and neutralized with distilled water. The material is centrifuged (3 minutes
187 at 1500 rpm), and the excess water is discarded. After decantation, the isolated kerogen
188 was sieved at 10 µm and strew slides were prepared for palynofacies analysis. This
189 analysis is based on the qualitative and quantitative (counting of a minimum of 300
190 particles) examination of the isolated kerogen using optical microscopy techniques
191 [transmitted white (TWL) and incident blue (fluorescence mode – FM) lights]. The
192 dispersed OM classification system adopted was proposed by Mendonça Filho and
193 Gonçalves (2017), Mendonça Filho et al. (2010b, 2012, 2014a, 2016) and Tyson (1995)
194 was used. Quantitative palynofacies data was normalized to percent composition.

195

196 3.2. *Organic petrography*

197 The organic petrologic analyses were performed at the Laboratory of Organic
198 Petrography of ICT – Instituto de Ciências da Terra (University of Porto, Portugal)
199 using a Leica DM4000 microscope equipped with a Discus-Fossil system in whole-rock
200 polished blocks prepared following ISO 7404-2 (2009). Identification of the organic
201 particles followed the morphology and optical properties described by Flores and
202 Suárez-Ruiz (2017) and Pickel et al. (2017).

203

204 3.3. *Geochemical analysis*

205 3.3.1. Total organic carbon and total sulfur

206 A LECO SC 144 analyzer (LAFO-UFRJ) was used for determination of total organic
207 carbon (TOC) and total sulfur (TS) contents (following removal of carbonates)
208 following NCEA-C-1282 (2002) and ASTM D4239-08 (2008). The mass percentage of
209 the sample not eliminated by the acid treatment was determined and is presented as
210 insoluble residue (IR).

211

212 3.3.2. Carbon isotopes

213 Isolated kerogen was used for δ¹³C determination in a carbonate-free fraction (δ¹³C_{Kerogen})
214 using a Flash EA 1112 Series elemental analyzer coupled online via a Finningan ConFlo
215 III interface to a Thermo Delta V S mass spectrometer. Analyses were performed at

216 MAREFOZ Laboratory (University of Coimbra, Portugal). Analytical precision is better
217 than $\pm 0.1\%$ for $\delta^{13}\text{C}$ (based on reference to an Acetanilide Standard from Thermo
218 Electron Corporation). A magnetic field separated gas species of different mass and
219 simultaneously measured by a Faraday cup collector array the isotopomers of CO_2 at m/z
220 44, 45, and 46.

221

222

223 3.3.3. Inorganic geochemistry

224 To corroborate the paleoenvironmental interpretation suggested by organic and
225 sedimentary field data, redox sensitive elements were used to estimate oxygenation and
226 productivity conditions at the sea floor. The assessment of redox conditions requires the
227 use of robust proxies such as Mn, U, V and Mo. U, V and Mo tend to be more soluble
228 under oxidizing conditions, and less soluble under reducing conditions, resulting in
229 authigenic enrichments in oxygen-depleted sediments. Mn has the reverse behavior,
230 displaying higher solubility under reducing conditions (Tribovillard et al., 2006).

231 Some redox sensitive elements are incorporated in the sediment mainly in association
232 with OM (Ni, Cu, Zn). After OM decay in reducing conditions, these elements co-
233 precipitate with sulfides. In consequence, these micronutrients (Calvert and Pedersen,
234 1993) are widely used to assess the organic C sinking flux, and, more usually, as
235 paleoproductivity proxies (e.g. Algeo and Maynard, 2004).

236 In this paper, the estimation of the oxygenation and productivity conditions at the sea
237 floor was based on geochemical data published by Fabre et al. (2018) for the Agadir
238 section, and Smrzka et al. (2017) for the Amma Fatma section. To highlight the
239 enrichment of each element from detrital background, enrichment factors (EF) with
240 respect to the Upper Continental Crust reference values (UCC; Wedepohl, 1995) were
241 calculated by the formula: $\text{EF}_X = (\text{X/Al})_{\text{sample}}/(\text{X/Al})_{\text{UCC}}$, where X is the element
242 considered and Al is used as a robust tracer of detrital input. Any relative enrichment
243 then is expressed by an $\text{EF} > 1$, whereas depleted elements have an $\text{EF} < 1$.

244

245 **4. Results and Interpretation**

246 *4.1. Agadir section*

247 4.1.1. Geochemical characterization

248 The Agadir section samples display a wide range of TOC contents, from 0.06 wt.% to
249 5.22 wt.%, with the highest average value being registered in the lower Turonian and

250 the lowest in upper Cenomanian. TS percentages range from 0.01 wt.% to 1.16 wt.%.
251 IR varies between <1 wt.% and 75 wt.%, showing similar concentrations in the upper
252 Cenomanian and lower Turonian (22 wt.% and 26 wt.%, respectively), with the lowest
253 values being recorded in the levels with lowest TOC content (Table 1).

254 Paleoredox proxies show the lowest average values during the upper Cenomanian (EFU
255 5.13, EFV 4.96, EFMo 3.33), with the exception of EFMn (7.26), while all
256 paleoproductivity proxies display averages <1. In the lower Turonian, U, V and Mo
257 exhibit a significant increase in EF (16.26, 42.50 and 55.19, respectively), while the
258 opposite occurs to EFMn (2.34). The paleoproductivity proxies follow the same trend,
259 with EFCu, EFNi and EFZn displaying a substantial increase during this interval (13.24,
260 2.26 and 25.73, respectively).

261 Due to the low OM content of some intervals at Agadir it was not possible to define a
262 $\delta^{13}\text{C}_{\text{Kerogen}}$ curve for the Agadir succession. Nevertheless, the analyzed samples show
263 the positive CIE with $\delta^{13}\text{C}_{\text{Kerogen}}$ values between -22.60‰ and -25.53‰ for the upper
264 Cenomanian, while the post-CIE values range from -26.88‰ and -27.71‰ during the
265 lower Turonian, in accordance with the intervals defined by Fabre et al. (2018) (Table
266 1). Although the $\delta^{13}\text{C}_{\text{Kerogen}}$ value of sample Ag40 is within the range of the ones
267 reported for OAE2 in other basins (see Erbacher et al., 2005; Barclay et al., 2010; Kuhnt
268 et al., 2017), it should be used with caution due to the low TOC content of the sample
269 (Table 1).

270

271 4.1.2. Kerogen characterization

272 Palynofacies analysis revealed the presence of components from all four kerogen
273 Groups; in all cases either the Amorphous or Palynomorph groups were dominant
274 (Table 1).

275 The Phytoclast Group was only identified in samples Ag10 and Ag40 in very small
276 percentages (0.3 %). This group is represented by brown non-opaque biostructured
277 phytoclasts (banded and pitted) under TWL, displaying dark brown to no fluorescence
278 (Fig. 3, A), and opaque phytoclasts (black under TWL and no fluorescence; Fig. 3, B).

279 The Amorphous Group is represented almost in its entirety by marine phytoplankton-
280 derived amorphous organic matter (AOM), with percentages varying from 0.3% to
281 97.0%. This component results from the microbiological reworking of marine
282 phytoplankton, and exhibits a heterogeneous texture and usual palynomorph inclusions,

283 alight to dark brown coloration under TWL, and light brown fluorescence (Fig. 3, C—
 284 H). Sample Ag97 shows AOM with oxidation features (variability in translucency and
 285 fluorescence color/intensity). In sample Ag102, a decrease in the degree of
 286 amorphization is responsible for an AOM with fluorescence colors varying from yellow
 287 to light brown (Fig. 3, G—H). Some resin particles were also observed at the base of the
 288 section (samples Ag10, Ag27 and Ag32).

289

290

291 Table 1. Organic geochemistry and palynofacies data of samples from the Agadir
 292 section.

Sample	Lithology	Geochemistry				Palynofacies			
		TOC (wt.%)	Sulfur (wt.%)	IR (wt.%)	$\delta^{13}\text{C}_{\text{Kerogen}}$ (‰)	PHY (%)	AMO (%)	PAL (%)	ZOO (%)
<i>Lower Turonian</i>									
Ag108	Calcareous Marl	4.56	0.68	39	-27.42	0.0	96.1	3.3	0.6
Ag102	Calcareous Marl	0.46	0.10	31	-27.71	0.0	93.1	5.8	1.1
Ag97	Marly Limestone	1.17	0.25	16	-	0.0	95.5	3.9	0.6
Ag91	Marly Limestone	5.22	1.16	22	-26.88	0.0	97.0	2.7	0.3
Ag56	Limestone	0.11	0.02	<1	-		Low Recovery		
<i>Upper Cenomanian</i>									
Ag52	Limestone	0.10	0.03	4	-		Low Recovery		
Ag51	Limestone	0.12	0.01	4	-		Low Recovery		
Ag40	Marly Limestone	0.17	0.03	18	-22.60	0.3	0.3	96.7	2.6
Ag32	Marl	0.44	0.08	75	-25.53	0.0	33.7	54.6	11.7
Ag27	Limestone	0.12	0.03	9	-	0.0	10.4	84.9	4.7
Ag10	Marl	0.47	1.15	71	-24.87	0.3	3.6	72.0	24.1
Ag6	Limestone	0.06	0.27	<1	-		Low Recovery		

293 TOC: Total organic carbon (wt.%); IR: Insoluble residue (wt.%); PHY: Phytoclast Group;

294 AMO: Amorphous Group; PAL: Palynomorph Group; ZOO: Zooclast Group.

295

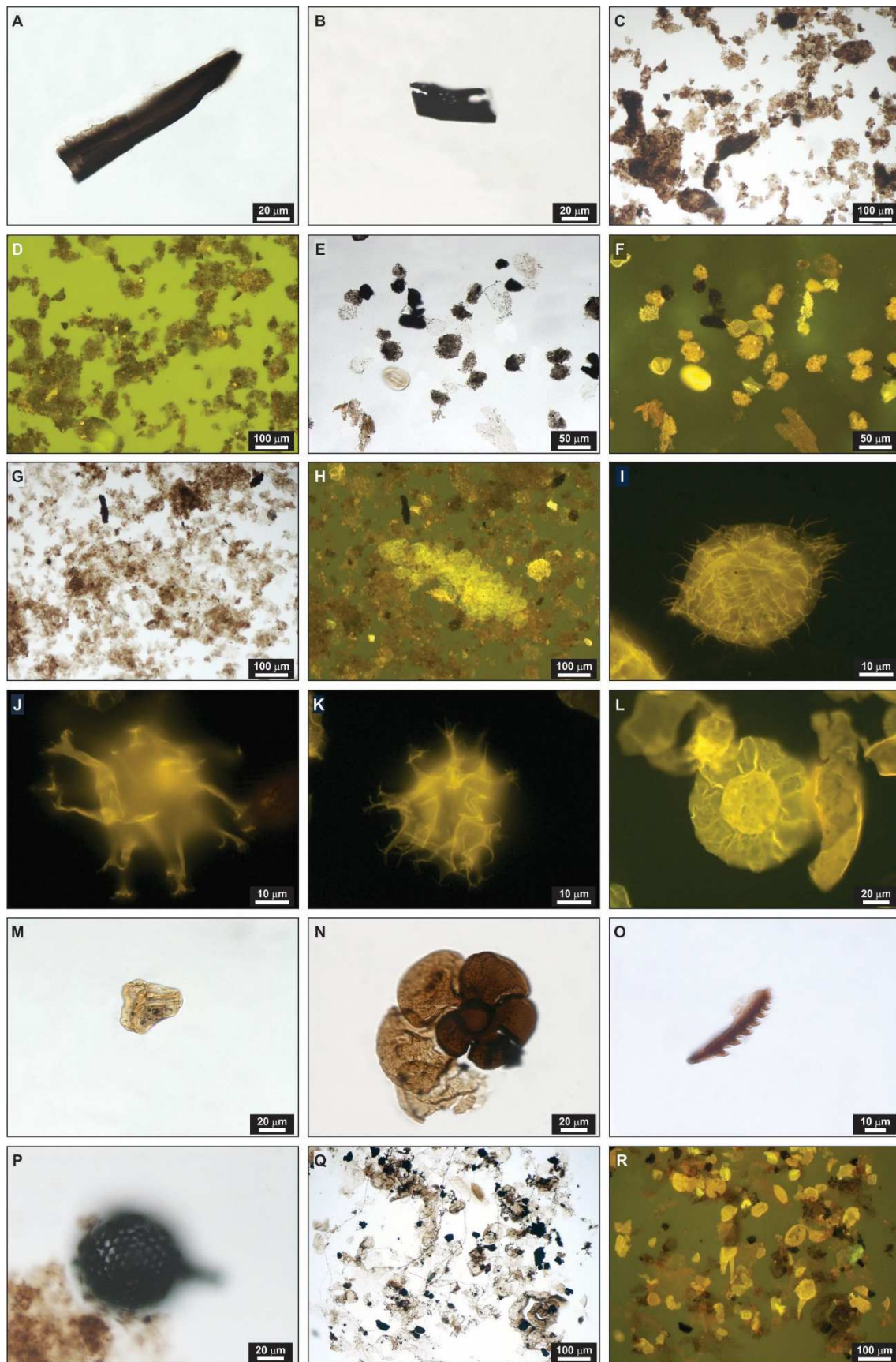
296 The Palynomorph Group is present in all samples showing a large variation between
297 2.7% and 96.7%. This group is represented by components of three subgroups: marine
298 microplankton, sporomorphs and zoomorphs. The marine microplankton subgroup is
299 the one present in highest percentages, and contains dinoflagellate cysts, acritarchs and
300 prasinophyte algae. Dinoflagellate cysts are the main marine component present in the
301 section, with percentages reaching 96.1% (Ag40). They are transparent to light brown in
302 TWL, and have strong greenish to yellow fluorescence (Fig. 3, I—K). Acritarchs
303 (samples Ag10, Ag27, Ag91 and Ag102) are transparent to light brown in TWL, exhibit
304 a yellow fluorescence, and are small in size with short processes. Prasinophyte algae,
305 namely from the genus *Pterospermella*, are present in samples Ag27, Ag32, Ag40 and
306 Ag108. These components are recognizable by their widely separated inner and outer
307 walls; the outer walls have alae, or flanges, that give a segmented appearance to some
308 specimens. These are light brown in TWL and have a strong yellow fluorescence.
309 *Pterospermella* specimens may appear whole or fragmented (Fig. 3, L). Pollen grains
310 and spores comprise the sporomorph subgroup. These palynomorph are light brown in
311 TWL and have yellow to orange fluorescence (Fig. 3, M). Sporomorphs in the samples
312 have a variety of different sizes, forms, and ornamentations. The zoomorph subgroup is
313 comprised of foraminiferal test-linings and scolecodonts. The foraminiferal test-linings
314 exhibit a light to dark brown color in TWL and no to brown fluorescence. They are
315 present in high percentages in sample Ag10 (19.9%) (Fig. 3, N). Scolecodonts show a
316 dark brown coloration under TWL and brown fluorescence (Fig. 3, O). The Zooclast
317 group is present throughout the section, with samples Ag10 and Ag32 displaying the
318 highest percentages (24.1% and 11.7%, respectively). This group is characterized by
319 undifferentiated zooclasts with light to dark brown color under TWL and no to dark
320 orange fluorescence, and crustacean eggs exhibiting a dark brown color in TWL and no
321 fluorescence.

322 Fungal remains, represented by spores and fungal hyphae (Tyson, 1995), are present in
323 high quantities in sample Ag10, and in smaller percentages in samples Ag32. These are
324 dark brown in TWL and do not fluoresce.

325 Pyritized radiolarians (Fig. 3, P) occur in samples Ag91 and Ag97 as both whole and
326 fragmented forms.

327 Samples Ag6, Ag51, Ag52 and Ag56 had low OM recovery, leading to insufficient
328 number of particles for palynofacies analysis.

329



330

331

332

333

Fig. 3. Photomicrographs of OM from the Agadir section samples. A: Non-opaque biostructured phytoclast (banded); B: Opaque phytoclast (pitted); C—F: Marine phytoplankton-derived AOM; G, H: Marine phytoplankton-derived AOM with lower

334 degree of amorphization; I—K: Dinoflagellate cysts; L: Prasinophyte algae,
335 *Pterospermella* sp.; M: Spore; N: Foraminiferal Test-Lining; O: Scolecodont; P:
336 Pyritized radiolarian; Q, R: Association of dinoflagellate cysts, foraminiferal test-linings
337 and fungal remains (Ag10). TWL: A—C, E, G, N—Q; Fluorescence mode: D, F, H—L,
338 R.

339

340 4.1.3. Paleoenvironmental reconstruction

341 The organic facies present in the Agadir sedimentary section were determined and the
342 succession was subdivided in five intervals for paleoenvironmental interpretation (Fig.
343 4).

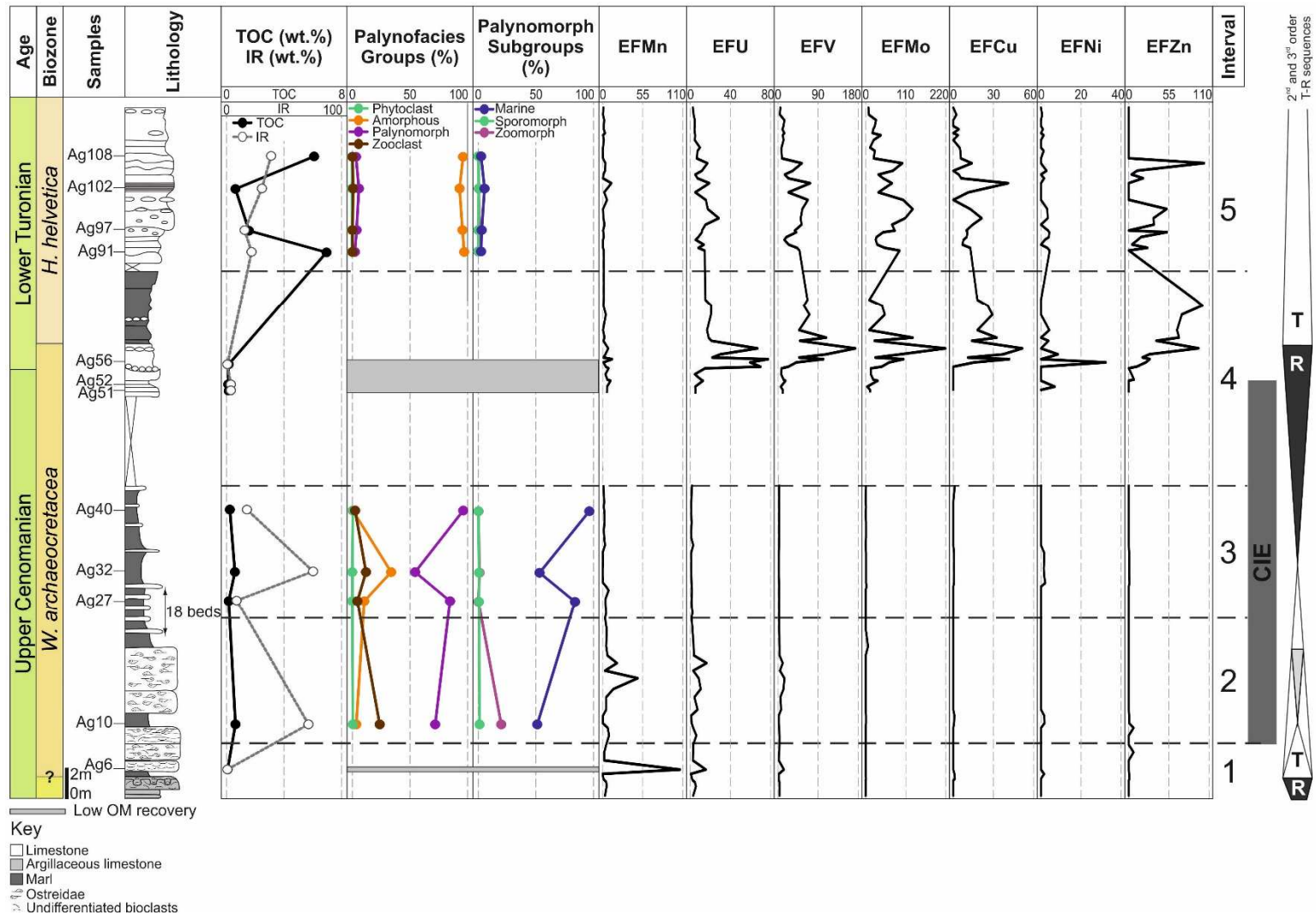
344 The base of the section, included in interval 1, represents the pre-CIE record and is
345 characterized by very low TOC content (<0.1 wt.%) and IR value (<1 wt.%), resulting
346 in low OM recovery. Inorganic proxies suggest oxic conditions (high EFMn, and low
347 EFMo) and low paleoproductivity (EFCu, EFNi and EFZn <1). This indicates that
348 deposition occurred in a very shallow high energy environment under oxic conditions
349 that did not favor OM preservation (Tyson, 1995; Mendonça Filho, et al., 2010b,
350 2014a).

351 Interval 2 encompasses the base of the CIE, displaying an increase in TOC content and
352 IR values coupled to an association co-dominated by marine microplankton,
353 foraminiferal test-linings and zooclasts, with high proportions of fungal remains (spores
354 and fungal hyphae) (Fig. 3, Q—R). This organic facies indicates an increase in water
355 level and decrease in energy of the system when compared to interval 1, and is usually
356 associated to upwelling areas (Tyson, 1995; Mendonça Filho, et al., 2010b, 2014a). This
357 seems to indicate an increase in nutrient availability that promoted primary productivity
358 (proliferation of marine microplankton) in an environment with normal oxygenation
359 conditions. A small peak in EFNi (up to 1.69) observed in sample Ag10 corroborates
360 the increase in paleoproductivity, while the oxic conditions are corroborated throughout
361 the interval by high EFMn and low EFMo.

362 The CIE record of interval 3 corresponds to a transgressive-regressive cycle defined by
363 the variations in TOC, IR and the amorphization degree of the marine microplankton
364 (concordant with 3rd order transgressive-regressive cycle previously proposed by
365 Lebedel, 2013). The palynofacies association is dominated either by marine
366 microplankton or by marine phytoplankton-derived AOM (Fig. 3, E—F). The increase
367 in water level culminates in sample Ag32, with the highest AOM values being coupled
368 to high TOC, high IR and low prevalence of continental components (Tyson, 1993,

1995; Mendonça Filho, et al., 2010b, 2014a). In terms of redox conditions, the increase in AOM indicates the occurrence of a dysoxic layer (decrease in EFMn) that promoted the amorphization of the marine microplankton possibly located inside the sediment or at the sediment-water interface, while the rest of the water column presented normal oxygen conditions allowing the development of benthic organisms (foraminiferal test-linings and scolecodonts) (Tyson, 1993, 1995; Mendonça Filho, et al., 2010b, 2014a). Low paleoproductivity conditions are suggested by low EFCu, EFNi and EFZn. The top of the CIE and base of the lower Turonian comprehended in interval 4, show very unfavorable conditions for OM preservation. The samples display very low TOC content (average 0.11 wt.%) and very low IR value (average 3 wt.%) that lead to low OM recovery. This indicates, similarly to interval 1, a very shallow high energy environment under oxic conditions, suggesting a decrease in water level from the top of interval 3 to interval 4 (Tyson, 1995; Mendonça Filho, et al., 2010b, 2014a). These conditions are not in accordance with the inorganic geochemical paleoredox proxies, possibly due to the presence of lag deposits in this stratigraphic level as described by Lebedel (2013). The majority of the lower Turonian is comprised in interval 5 and is characterized by a significant increase in TOC (average 2.85 wt.%) and slight increase in IR (average 27 wt.%) related to the increase of biogenic silica (Lebedel, 2013). This is coupled to a palynofacies association dominated, almost entirely, by marine phytoplankton-derived AOM, suggesting a transgressive trend for the lower Turonian [concordant with Lebedel (2013) interpretations]. This increase in TOC and degree of amorphization was promoted by the implementation of reducing conditions (high EFU, EFV and EFMo), favoring OM preservation, and allowing the anaerobic microbiological reworking of the marine microplankton (Tyson, 1993, 1995; Mendonça Filho, et al., 2010b, 2014a; Mendonça Filho and Gonçalves, 2017). This layer with low oxygen availability (dysoxic to anoxic conditions), similarly to interval 3, is probably located at the sediment-water interface due to the occurrence of both pelagic and benthic organisms (foraminiferal test-linings, crustacean eggs, radiolarians). High primary productivity is also suggested by an increase in EFCu, EFNi and EFZn. The oxidation features identified in the AOM of sample Ag97 can be explained by a higher alkalinity of the system suggested by a decrease in IR. The decrease in the degree of amorphization observed in sample Ag102 could suggest a slight decrease in water column, associated

402 to a slight decrease in the reducing conditions (Tyson, 1993, 1995; Mendonça Filho, et
403 al., 2010b, 2014a; Mendonça Filho and Gonçalves, 2017).



404
405
406

Fig. 4. Geochemical and palynofacies data stratigraphic variation across the upper Cenomanian—lower Turonian interval of the Agadir section. EF calculated based on Fabre et al. (2018) geochemical data. 2nd and 3rd order T-R sequences according to Lebedel (2013).

407 4.2. *Amma Fatma section*

408 4.2.1. Geochemical characterization

409 The Amma Fatma samples display high organic richness, with TOC content ranging
410 from 3.26 wt.% to 7.52 wt.%. This is accompanied by TS values varying from 0.62
411 wt.% and 1.56 wt.% and a mostly carbonate sediment, with IR ranging from 11 wt.% to
412 42 wt.% (Table 2). It is important to note that these IR values may actually be higher
413 due to the presence of salts identified during the polishing process of the whole-rock
414 blocks. Nevertheless, similar CaCO₃ contents are described by El Albani et al. (2001)
415 and Smrzka et al. (2017) for the black shales at Amma Fatma, and by Einsele and
416 Wiedmann (1982) and Ghassal et al., (2016) for the lower Turonian black shales of the
417 Tarfaya Basin. In these related studies, the same correlation between carbonate content
418 and TOC content is observed.

419 Inorganic geochemical proxies are uniform throughout the section, and have low EFMn
420 (<1), and high EFU, EFV and EFMo (22.15, 24.40, 96.17). EFCu, EFNi and EF Zn
421 show high values throughout the section (7.29, 22.70 and 18.64, respectively).

422 $\delta^{13}\text{C}_{\text{Kerogen}}$ displayed values ranging from -27.35‰ and -28.23‰ for the lower Turonian
423 succession (Table 2). These values are comparable to those published by Smrzka et al.
424 (2017), supporting the assertion that these sediments were deposited following the
425 OAE2 in the Tarfaya Basin.

426

427 Table 2. Organic geochemistry and palynofacies data of samples from the Amma Fatma
 428 section.

Sample	Lithology	Geochemistry				Palynofacies			
		TOC (wt.%)	Sulfur (wt.%)	IR (wt.%)	$\delta^{13}\text{C}_{\text{Kerogen}}$ (‰)	PHY (%)	AMO (%)	PAL (%)	ZOO (%)
AF18	Marly Limestone	4.66	0.98	23	-28.00	0.0	97.3	1.4	1.4
AF17	Marly Limestone	7.14	1.19	17	-27.43	0.0	98.8	0.6	0.6
AF16	Marly Limestone	3.36	0.62	14	-	0.0	96.5	2.0	1.4
AF15	Marly Limestone	5.85	1.08	18	-	0.0	96.6	1.9	1.6
AF14	Marly Limestone	4.04	0.62	18	-28.01	0.0	97.9	2.1	0.0
AF13	Marly Limestone	4.77	0.71	32	-	0.0	98.9	1.1	0.0
AF12	Marly Limestone	5.86	1.14	23	-27.73	0.0	99.4	0.3	0.3
AF11	Marly Limestone	5.50	0.88	13	-27.54	0.0	99.7	0.3	0.0
AF10	Marly Limestone	6.37	1.24	24	-28.23	0.0	99.5	0.3	0.3
AF9	Marly Limestone	7.52	1.56	29	-27.93	0.0	98.3	1.4	0.3
AF8	Marly Limestone	3.26	0.91	24	-27.80	0.0	98.7	0.7	0.7
AF7	Marly Limestone	4.57	0.76	11	-28.06	0.0	99.4	0.0	0.6
AF6	Marly Limestone	4.99	0.97	24	-27.99	0.0	98.7	0.7	0.7
AF5	Marly Limestone	6.65	0.99	20	-27.79	0.3	99.3	0.3	0.0
AF4	Marly Limestone	5.18	1.44	33	-27.59	0.0	97.8	2.0	0.2
AF3	Marly Limestone	4.93	1.21	35	-27.92	0.0	98.5	0.9	0.6
AF2	Marly Limestone	6.08	1.08	32	-27.35	0.0	99.5	0.5	0.0
AF1	Marl	5.29	1.42	42	-27.58	0.0	99.7	0.3	0.0

429 TOC: Total organic carbon (wt.%); IR: Insoluble residue (wt.%); PHY: Phytoclast Group;
 430 AMO: Amorphous Group; PAL: Palynomorph Group; ZOO: Zooclast Group.

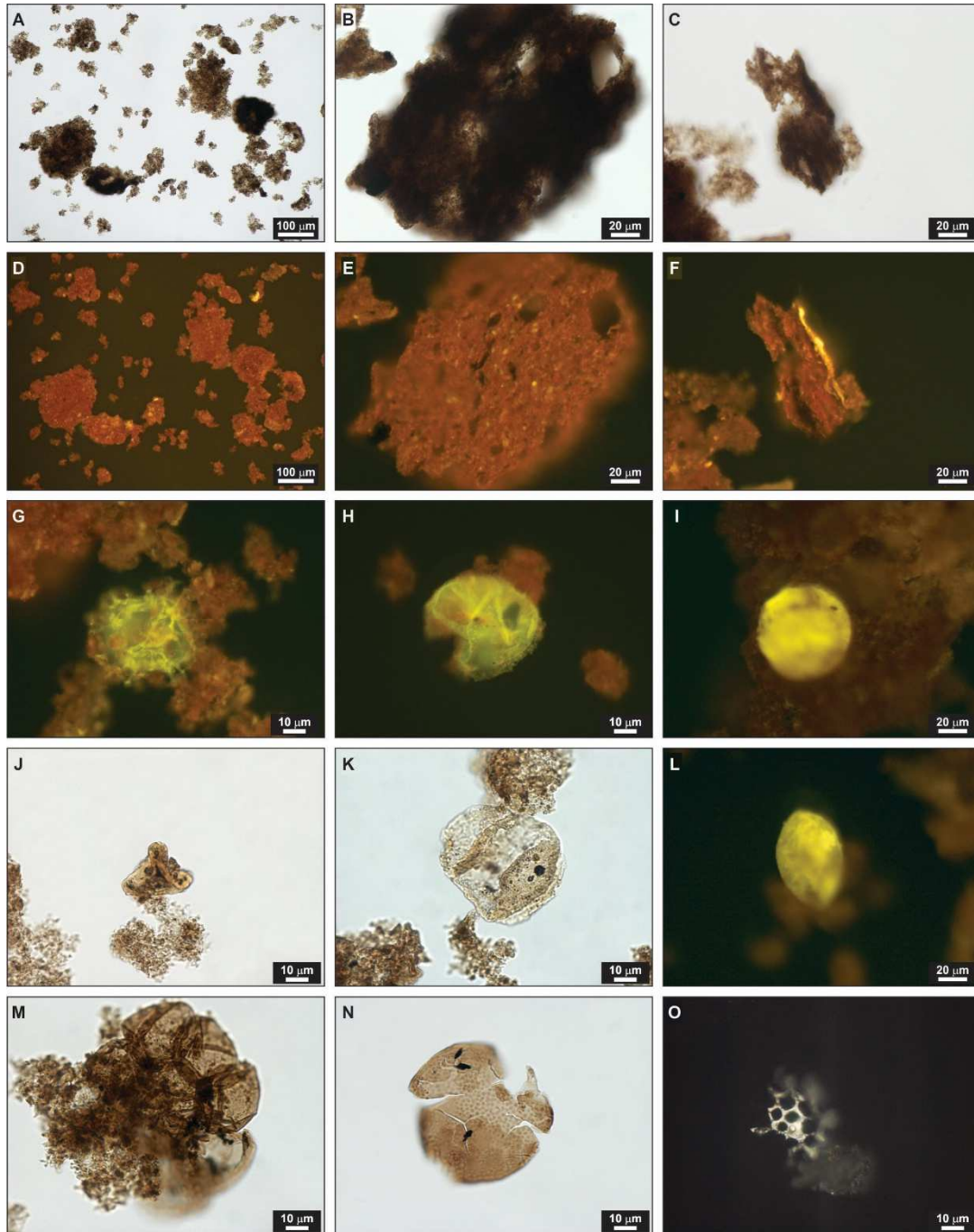
431

432 4.2.2. Kerogen characterization

433 The kerogen is characterized, almost entirely, by components from the Amorphous
 434 Group (Table 2). This group is represented by bacterial-derived AOM that is dark
 435 brown in TWL and orange to reddish, sometimes yellow, in fluorescence mode (Fig. 5,
 436 A—F). The AOM is dense and displays an amorphous and pitted aspect due to the

437 impression of the carbonate minerals following dissolution with HCl (Fig. 5, B—C, E—
438 F). Under RWL, bituminite occurs under the form of laminae surrounding and being
439 closely associated with the calcareous mineral matrix, and presents an orange to reddish
440 fluorescence color, features that suggest a bacterial origin (Glikson and Taylor, 1986;
441 Pickel et al., 2017, and references therein; Fig. 6, A—B). Lamalginite, zooclasts,
442 dolomite rhombohedrons and pyrite framboids were also observed (Fig. 6).
443 The Phytoclast Group displays small percentages, appearing only in sample AF5. Only
444 non-opaque biostructured phytoclasts (NOB) displaying a brown color under TWL and
445 no fluorescence were identified, namely pitted and banded NOB phytoclasts.
446 Components from the Palynomorph Group are also present in small percentages,
447 namely from the marine microplankton, sporomorph, freshwater microplankton and
448 zoomorph subgroups. The marine microplankton subgroup is characterized by
449 dinoflagellate cysts, acritarchs and prasinophyte algae (*Tasmanites* and *Pterospermella*
450 species). The dinoflagellate cysts are transparent to very light brown in TWL and
451 present a strong yellow fluorescence, occurring mostly surrounded by AOM (Fig. 5,
452 G—H). Acritarchs are very small sized, with small processes, and are transparent to
453 very light brown color in TWL with strong yellow fluorescence. Prasinophyte algae
454 exhibit a light brown color in TWL and a yellow fluorescence (Fig. 5, I). The
455 sporomorph subgroup is characterized by spores and pollen grains displaying a light
456 brown to brown color in TWL and a yellow fluorescence (Fig. 5, J). Pollen grains in the
457 form of agglomerates in samples AF12 and AF14 and bisaccate pollen in sample AF6
458 were also identified (Fig. 5, K). The freshwater microplankton subgroup is present in
459 sample AF2, being represented by Zygnemataceae specimens (*Spirogyra* genus)
460 exhibiting a transparent to very light brown color in TWL and a yellow fluorescence
461 (Fig. 5, L). The zoomorph subgroup is represented by foraminiferal test-linings
462 displaying a brown color under TWL and no fluorescence; some have sulfide inclusions
463 (Fig. 5, M).
464 Other minor components were also identified throughout the section, including
465 crustacean eggs (Fig. 5, N) and undifferentiated zooclasts exhibiting a dark brown color
466 in TWL and no fluorescence, resin particles with a hyaline aspect, and fragments of
467 pyritized radiolarians (Fig. 5, O).

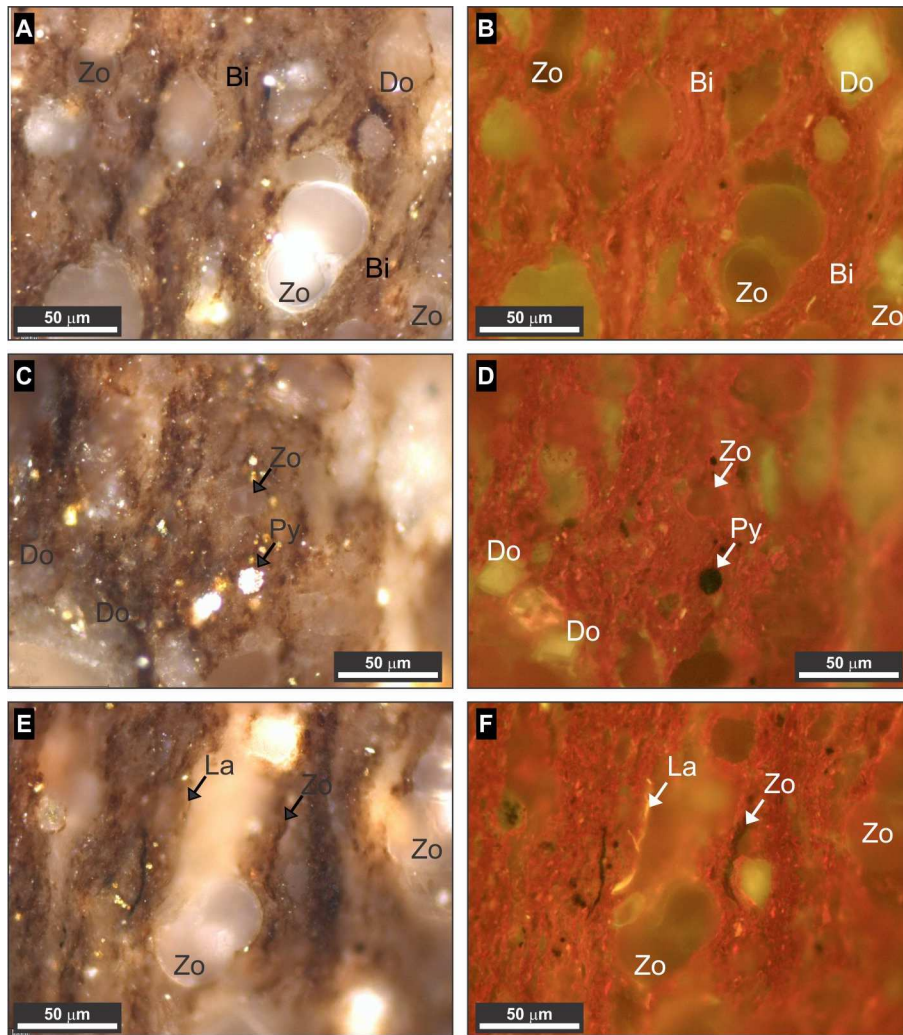
468



469

470 Fig. 5. Photomicrographs of OM from the Amma Fatma section samples. A—F:
 471 Bacterial AOM; G, H: Dinoflagellate cyst; I: Prasinophyte algae, *Tasmanites* genus; J:
 472 Spore; K: Bisaccate pollen grain; L: - Zygmemataceae from the genus *Spirogyra*; M:
 473 Foraminiferal Test-Lining; N – Crustacean egg; O: Fragment of pyritized radiolarian.
 474 TWL: A—C, J—K, M—N; FM: D—I, L; RWL: O.

475



476

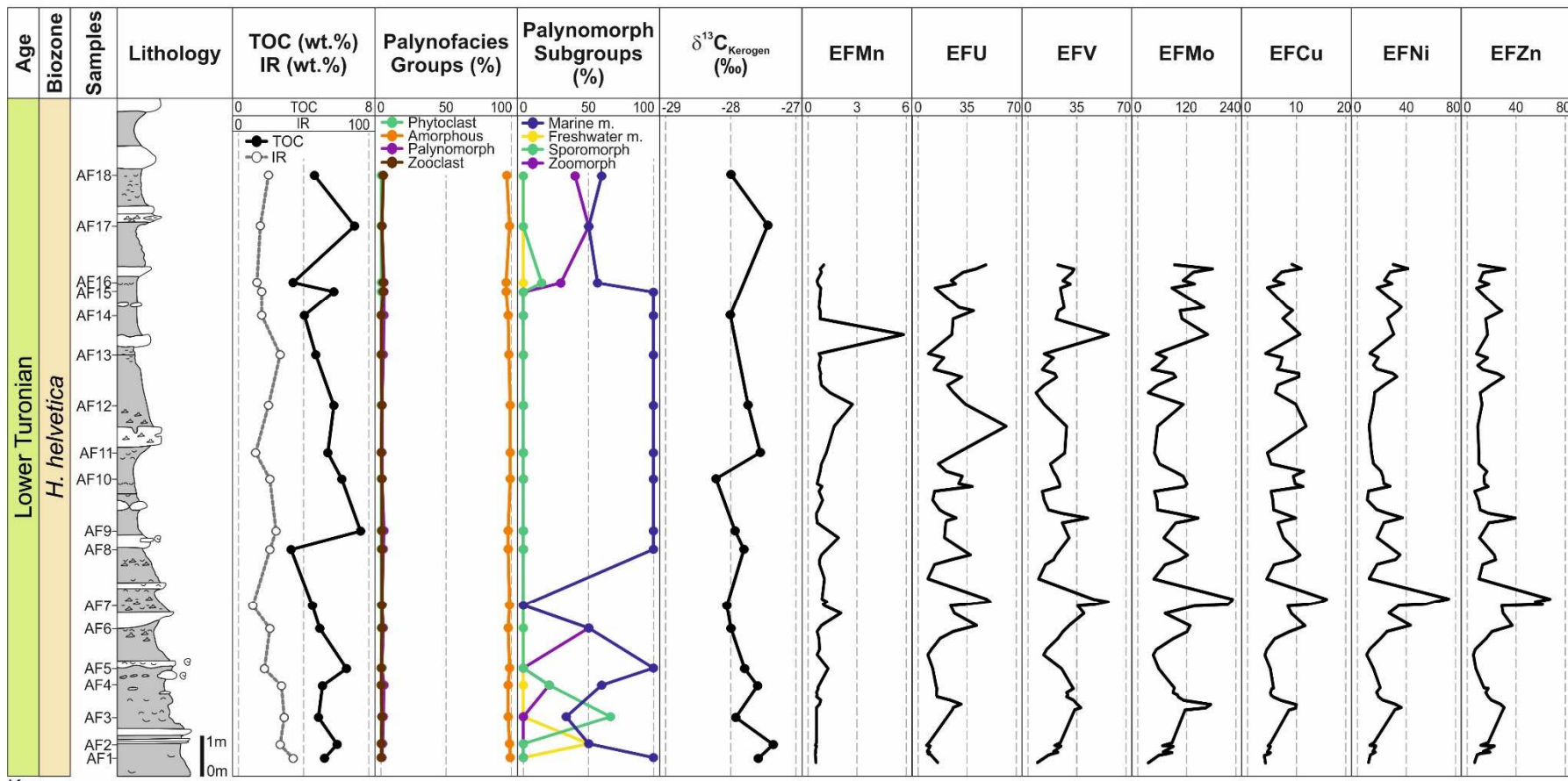
477 Fig. 6. Photomicrographs of whole-rock polished blocks from the Amma Fatma section
 478 samples. Bi: Bituminite; Do: dolomite rhombohedron; La: lamalginite; Py: pyrite
 479 framboid; Zo: zooclast. RWL: A, C, E; FM: B, D, F.

480

481 4.2.3. Paleoenvironmental reconstruction

482 The organic facies of the lower Turonian of the Amma Fatma section is homogeneous
 483 throughout the sedimentary succession (Fig. 7). It is represented by a palynofacies
 484 association dominated by bacterial AOM. The bacterial material is derived from
 485 autotrophic-photosynthetic bacteria that produced a bacterial mucilage usually
 486 associated to carbonate sediments (Tyson, 1995; Mendonça Filho et al., 2010a; 2010b,
 487 2014a; Mendonça Filho and Gonçalves, 2017). This mucilage, the Extracellular
 488 Polymeric Substance (EPS), is mainly produced by cyanobacteria (blue-green algae)
 489 and thiobacteria (sulfur bacteria) that do not fossilize as recognizable entities (Tyson,
 490 1995; Mendonça Filho et al., 2010a, 2010b, 2014a; Mendonça Filho and Gonçalves,
 491 2017). In this case, this dense bacterial AOM results from the microbiological

492 reworking of the EPS (produced by the autotrophic bacteria) by heterotrophic bacteria
493 colonies under reducing conditions (Mendonça Filho et al., 2010a, 2010b, 2014a;
494 Mendonça Filho and Gonçalves, 2017). High percentages of this bacterial material are
495 usually associated with high TOC contents, as is the case in Amma Fatma. The type of
496 AOM and its relationship with the mineral matrix, the palynofacies association with the
497 presence of continental components (including freshwater microplankton and pollen
498 grain agglomerates), and the high TOC content coupled with the low IR values indicate
499 that sedimentation occurred in a shallow marine environment (shelf environment), with
500 some degree of restriction, under reducing conditions and with high primary
501 productivity (Tyson, 1995; Mendonça Filho et al., 2010a, 2010b, 2014a). These
502 conditions are further corroborated by a significant enrichment in paleoredox (EFU,
503 EFV and EFMo > 1) and productivity (EFCu, EFNi and EFZn > 1) chemical proxies.



- Key
- Limestone
 - ▒ Argillaceous limestone
 - ▒ Undifferentiated bioclasts
 - ⊖ Bivalve
 - ⊙ Ammonite
 - ⊚ *Thalassinoides*

504

505 Fig. 7. Geochemical and palynofacies data stratigraphic variation across the lower Turonian of the Amma Fatma section. EF calculated based on
 506 Smrzka et al. (2017) geochemical data.

507 **5 Discussion**

508 *5.1. Organic matter origin*

509 The upper Cenomanian—lower Turonian interval shows a significant OM variability in
510 terms of composition, evolution and concentration, in space and time, along the
511 Moroccan coast. The organic concentration is high in the Tarfaya area and increases
512 significantly in the Agadir section during the lower Turonian, although staying, in
513 average, lower than in the Amma Fatma section. The OM associations of the Agadir
514 section display the dominance of marine OM components, showing differences of
515 degree of amorphization, while in Tarfaya the sequence is dominated by bacterial-
516 derived AOM.

517 The Cenomanian organic association at Agadir is co-dominated, at the base (sample
518 Ag10), by marine microplankton, foraminiferal test-linings and zooclasts. This is
519 followed by an association dominated by marine microplankton with low percentages of
520 marine phytoplankton-derived AOM (Fig. 8). At Tarfaya, the Cenomanian—Turonian
521 sequence seems to be fairly consistent in terms of OM origin. In fact, the OM
522 association identified in this study in the lower Turonian of Amma Fatma (Tarfaya
523 Basin) is similar to the Cenomanian association of the same basin described in the
524 literature, with the dominance of the bituminite maceral and reddish-brown gelified
525 AOM in isolated kerogen (Kolonic, 2002; Nzoussi-Mbassani et al., 2005; Prauss, 2012;
526 Fig. 8). Kolonic et al. (2002) indicate a type I and II kerogen for the Cenomanian of the
527 Tarfaya Basin (Mohammed Plage section and S75 borehole; Fig. 1), a high
528 concentration of S in the OM (determined by SEM-EDS) and sulfur/carbon ratio > 0.36
529 (Nzoussi-Mbassani et al., 2005), suggesting a mixed contribution of marine and
530 bacterial OM with euxinic conditions in the water column (Fig. 8). Furthermore, these
531 authors suggest that OM natural sulfurization must have played a key role in the
532 preservation of the high quantities of OM present in the Cenomanian—Turonian
533 sediments of this basin, a fact later confirmed by Raven et al. (2019).

534 During the Turonian, with the establishment of dysoxic to anoxic conditions in the
535 water column at Agadir, the marine components display a high degree of amorphization,
536 with the association being dominated by marine phytoplankton-derived AOM (kerogen
537 type II; Gertsch et al., 2010; Fig. 8). This differs from the Tarfaya Basin, where the
538 dominance of bacterial material is in accordance with the high hydrogen index
539 determined for lower Turonian sediments of Amma Fatma (El Albani et al., 2001) and
540 of the Tarfaya S4 borehole (Ghassal et al., 2016) (reaching values > 800 mg HC/g TOC

541 - kerogen type I and II; Fig. 1, 8). The same evidences have been described for the black
542 shales of the *H. helvetica* biozone of the S75 borehole by Kolonic et al. (2002) (Fig. 1,
543 8). Furthermore, a high methylated hopanes/hopanes ratio was determined by Ghassal et
544 al. (2016) in the lower Turonian of S4 borehole, suggesting a high bacteria and
545 cyanobacteria contribution (Summons et al., 1999; Kuypers et al., 2004b; Peters et al.,
546 2005; Ricci et al., 2014).

547 The molecular analysis of the S75 borehole displayed high concentrations of neohop-
548 13(18)-ene (an indicator of a stratified water body, Peters et al., 2005) accompanied by
549 the presence of isorenieratane derivatives (Kolonic et al., 2002; Fig. 1, 8). Isorenieratane
550 is a carotenoid pigment only biosynthesized by the brown strain of green sulfur bacteria
551 (*Chlorobiaceae*; Sinninghe Damsté et al., 1993; Madigan et al., 2015). These bacteria
552 are strict anoxygenic photolithoautotrophs and require the simultaneous presence of
553 sulfide and light to carry out photosynthesis, with the molecular fossil remains of their
554 specific carotenoids (isorenieratene and chlorobactene) being considered indicators of
555 photic zone anoxia in marine environment (Sinninghe Damsté et al., 1993; van
556 Gemerden and Mas, 1995; Marschall et al., 2010). These conditions are observed in
557 some present day analogs, namely in the Black Sea, where green sulfur bacteria thrive at
558 about 100 m depth in extreme low-light conditions near the chemocline (van Gemerden
559 and Mas, 1995; Marschall et al., 2010).

560 The identification of isorenieratane derivatives corroborates therefore, not only the
561 establishment of euxinic conditions in the photic zone during the deposition of the lower
562 Turonian black shales in the Tarfaya Basin, but also the development of this green
563 sulfur bacterial biomass (Sinninghe Damsté et al., 1993; Sinninghe Damsté and Köster,
564 1998; Kolonic et al., 2002; Marschall et al., 2010; Smrzka et al., 2017). Furthermore, in
565 upwelling sediments, as is the case of the Amma Fatma black shales, the organic
566 association is usually entirely or predominantly constituted by marine planktonic and
567 bacterial material (e.g. Summerhayes, 1983; ten Haven et al., 1990; Tyson, 1995;
568 Carvalho and Rodriguez, 2004; Lavik et al., 2008; Bertagnolli et al., 2011). These
569 evidences are completely in accordance with the type of AOM identified at Amma
570 Fatma. The reddish fluorescence of this OM may be related to natural OM sulfurization
571 (dominance of sulfur compounds in the kerogen), as described by Stankiewicz et al.
572 (1996), being also important to take into account the role of this process in the
573 deposition of these hydrogen-rich sediments (Kolonic et al., 2002).

578 5.2. Paleoenvironmental conditions and sea level evolution during the Cenomanian—
579 Turonian interval

580 The variability of the organic facies previously mentioned suggests spatio-temporal
581 paleoenvironmental variations.

582 The *R. cushmani*/*W. archaeocretacea* biozone boundary in the Agadir area is marked by
583 an exposure surface (Jati et al., 2010) followed, at the base of the *W. archaeocretacea*
584 biozone, by sedimentation in a shallow high energy environment, with oxic conditions
585 not allowing the preservation of OM (prior to CIE). These oxidizing conditions are in
586 accordance with published Rock-Eval data showing low hydrogen index coupled to
587 very high oxygen index values (Type IV kerogen; Gertsch et al., 2010; Fig. 8). At
588 Tarfaya, the late Cenomanian is characterized by a major sea level rise suggested by
589 decreasing detrital input and increasing hydrogen index, although a short low-amplitude
590 sea level fall occurs prior to CIE (Gale et al., 2002, 2008; Gertsch et al., 2010). At the
591 Mohammed Beach reference section (located ~ 21 km NE of Amma Fatma; Fig. 1),
592 deposition occurred in a middle shelf environment with a carbonate dominated system
593 with redox conditions becoming more anoxic to the top (Kuhnt et al., 2005, 2009; Mort
594 et al., 2008; Gertsch et al., 2010; Ghassal et al., 2016)

595 The CIE is marked, at Agadir, by a 3rd order transgressive-regressive cycle, represented,
596 at the base, by a shallow environment with an increase in primary productivity under
597 normal oxygenation conditions (corroborated by an Ostreidae biostrome), followed by
598 an increase in water level associated to a decrease in oxygen availability, promoting the
599 amorphization of the marine microplankton. Benthonic and planktonic foraminiferal
600 assemblages, rare prior to CIE, increase in abundance and diversity during the CIE,
601 consisting mainly of low oxygen-tolerant species (e.g. *Coryphostoma plaitum*,
602 *Gavelinella sandidgei*, *Neobulimina albertensis* and *Pyraminida Prolixa*; Gertsch et al.,
603 2010), corroborating an increase in water level, and dysoxic bottom waters with
604 stratification of the water column. The decrease of AOM to the top of the CIE indicates
605 a decrease in water level and an increase in oxygen availability. This regressive trend
606 culminates in the erosive emersion surface observed at the top of the upper Cenomanian
607 (this surface truncates bioclastic bioturbated wackestones that follow sandstone beds,
608 with quasi-planar lamination or hummocky cross-stratification, with wave ripples at the
609 top interpreted as storm beds; Jati et al., 2010). The topmost upper Cenomanian and
610 base of the lower Turonian is therefore characterized by a shallow high energy
611 environment, with high oxygen availability.

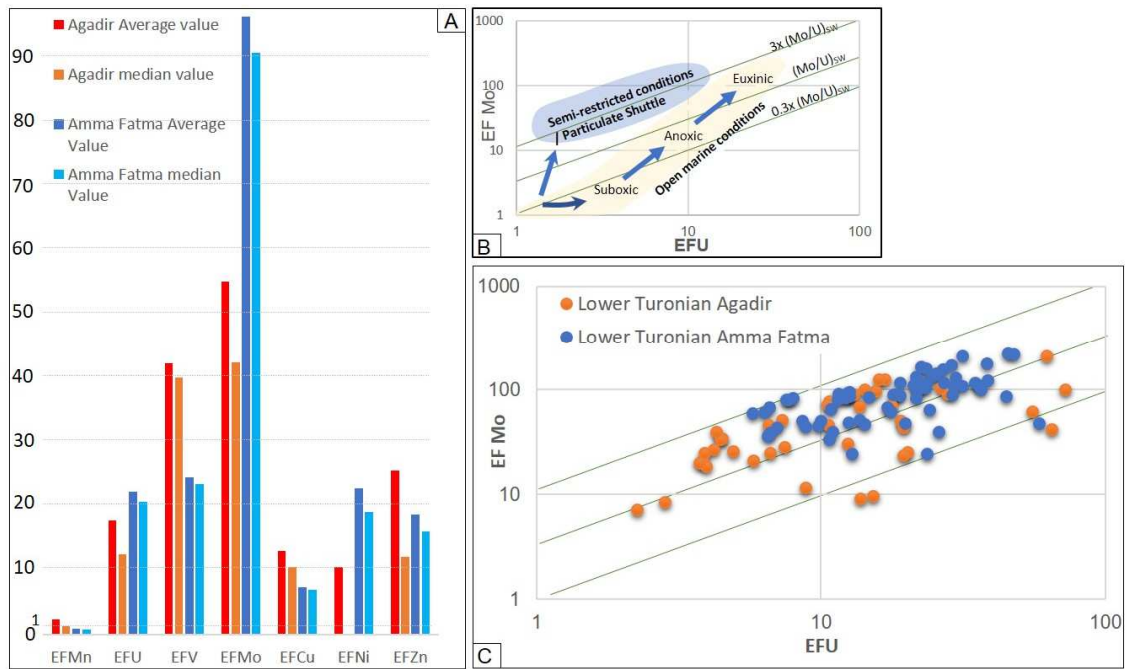
612 During CIE at Tarfaya Basin, deposition occurs under anoxic/euxinic conditions, with
613 high primary productivity favoring the preservation of OM of marine origin, that is, a
614 mixture of marine microplankton and both bacteria and cyanobacteria (TOC up to ~15
615 wt.%; Gertsch et al., 2010; Ghassal et al., 2016).

616 During the lower Turonian, a sedimentary homogenization along the Moroccan coast is
617 suggested by sedimentological data (e.g. El Albani et al., 1999b; Lüning et al., 2004;
618 Gertsch et al., 2010; Jati et al., 2010) which is in agreement with the inorganic
619 geochemical data (Fig. 9). Figure 9A allows the comparison between the average and
620 median enrichment factor values of the main paleoredox and paleoproductivity proxies,
621 suggesting similar conditions for both sections. These trace metal enrichments are in the
622 same order of magnitude as those recorded in coastal upwelling and Cenomanian—
623 Turonian black shales (Brumsack, 2006). The concomitant enrichment in U, V and Mo
624 in these sediments reflects euxinic conditions at the sediment-water interface or in the
625 water column (Algeo and Maynard, 2004; Tribovillard et al., 2004), while a significant
626 enrichment in Cu, Ni and Zn suggests high paleoproductivity (meso- to eutrophic
627 conditions).

628 The covariation of EFU and EFMo in sediments is considered a tool to evaluate the
629 degree of restriction of a basin (semi-restricted basin versus unrestricted marine
630 environment, Fig. 9, B). This is related to the different geochemical behaviors of Mo
631 and U under anoxic conditions (for more detail see Algeo and Tribovillard, 2009;
632 Tribovillard et al., 2012).

633 A similar distribution of the lower Turonian samples of Agadir and Amma Fatma is
634 observed in the EFMo versus EFU diagram of figure 9C, suggesting equivalent
635 hydrographic conditions. These data encompass the present-day seawater Mo/U ratio,
636 reflecting environmental conditions of two coastal basin environments with mainly
637 open marine conditions (Fig. 9, B; Tribovillard et al., 2012) which fluctuate between
638 euxinic and suboxic seafloor conditions (Dickson et al., 2016). The same conditions are
639 recorded for the upper Cenomanian—Turonian interval of the S57 drill core in the
640 Tarfaya Basin (Dickson et al., 2016), reflecting stability of the environmental context
641 during the upper Cenomanian—Turonian interval at Tarfaya, while reducing conditions
642 only develop during the lower Turonian in the Agadir Basin.

643
644



645

646 Fig. 9. Inorganic geochemistry data. A: Average and median enrichment of the main
 647 paleoredox (Mn, U, V and Mo) and paleoproductivity (Cu, Ni, Zn) proxies for the lower
 648 Turonian of the Agadir and Amma Fatma sections. B: EFMo versus EFU with
 649 hydrographic conditions according to Tribovillard et al. (2012). Diagonal green lines
 650 represent 3/1; 1/1 and 0.3/1 (Mo/U) ratios of present-day seawater. Blue area
 651 corresponds to weakly restricted basins with “Particulate Shuttle” effect. Yellow area
 652 shows EFMo versus EFU evolution under suboxic to euxinic conditions in modern open
 653 marine environments (Tribovillard et al., 2012). C: EFMo versus EFU for the lower
 654 Turonian of the Agadir and Amma Fatma samples.

655

656 Although sedimentological and inorganic geochemical data indicate similar depositional
 657 conditions at both studied locations, the organic facies suggest slightly different
 658 contexts and conditions at the time of deposition of these organic-rich deposits. Thus, in
 659 the Agadir area, the lower Turonian is marked by an overall transgressive trend with the
 660 establishment of dysoxic to anoxic conditions. Short-term water level oscillations are
 661 indicated by different degrees of amorphization of the marine microplankton (Type II
 662 kerogen - Gertsch et al., 2010). These depositional conditions are corroborated by
 663 foraminiferal assemblages, with fluctuations of the oxygen concentration being already
 664 suggested by Jati et al. (2010) based on changes in planktonic/total foraminifera ratio.

665

666 In the Tarfaya Basin, the OM assemblage suggests that the depositional environment is
667 characterized by a shallow water column (shelf environment) with O₂ stratification,
668 euxinic conditions, and some degree of restriction, in order to allow the proliferation of
669 the bacterial biomass. The higher Mo enrichment at Amma Fatma suggests more
670 sulfidic (or sulfate-reducing) conditions, probably due to the presence of free H₂S in the
671 water column only in this area (Fig. 9, A). This could explain the highest OM
672 concentration in the Amma Fatma section as it could provide better conditions for OM
673 preservation. Periodic reoxygenation of the water column and bottom waters is
674 indicated by the presence of *Thalassinoides* (Fig. 2, B). These periods of higher
675 oxygenation were not possibly to identify with the resolution of the sampling, although,
676 some levels with lower TOC are described for the lower Turonian of the Tarfaya Basin
677 by Kolonic et al. (2002).

678 According to Haq (2014), the earliest Turonian characterized the maximum of this sea-
679 level rise, and Einsele and Wiedmann (1982) suggest a deep shelf sea with water depth
680 being controlled by the global sea-level rise and the difference between accumulation
681 rate and subsidence. Other studies demonstrated that sea-level increased continuously
682 during the Cenomanian, promoted by this combination of eustatic global sea-level rise
683 and shelf subsidence (Gebhardt et al., 2004; Mort et al., 2008; Kuhnt et al., 2009). In the
684 Tarfaya Basin, the lithofacies and the biofacies distribution during the Late Cretaceous
685 suggest a maximum depth of 200 m (Kuhnt and Wiedmann, 1995; El Albani et al.,
686 1999a). El Albani et al (1999b), in a sedimentological study of storm deposits at Amma
687 Fatma, defined that these lower Turonian sediments are deposited on a platform with an
688 estimated palaeobathymetry during the lower Turonian fluctuating between 100–150
689 m depth. This interpretation seems to be in accordance with a shallow water with high
690 productivity realm in an outer shelf setting proposed for the deposition of the Amma
691 Fatma organic-rich deposits by Smrzka et al. (2017), based on foraminiferal and clay
692 assemblages, which is corroborated by the organic facies defined in this study (see
693 section 4.2.3 and 5.1).

694

695 *5.3. Paleoproductivity vs upwelling*

696 During the lower Turonian, reducing conditions persisted in the Tarfaya Basin and
697 developed in the Agadir Basin associated to an increase in paleoproductivity (Einsele
698 and Wiedmann, 1982; Mort et al., 2008; Fabre et al., 2018). The high paleoproductivity
699 in the northwest African shelf, suggested by inorganic geochemical data, is considered

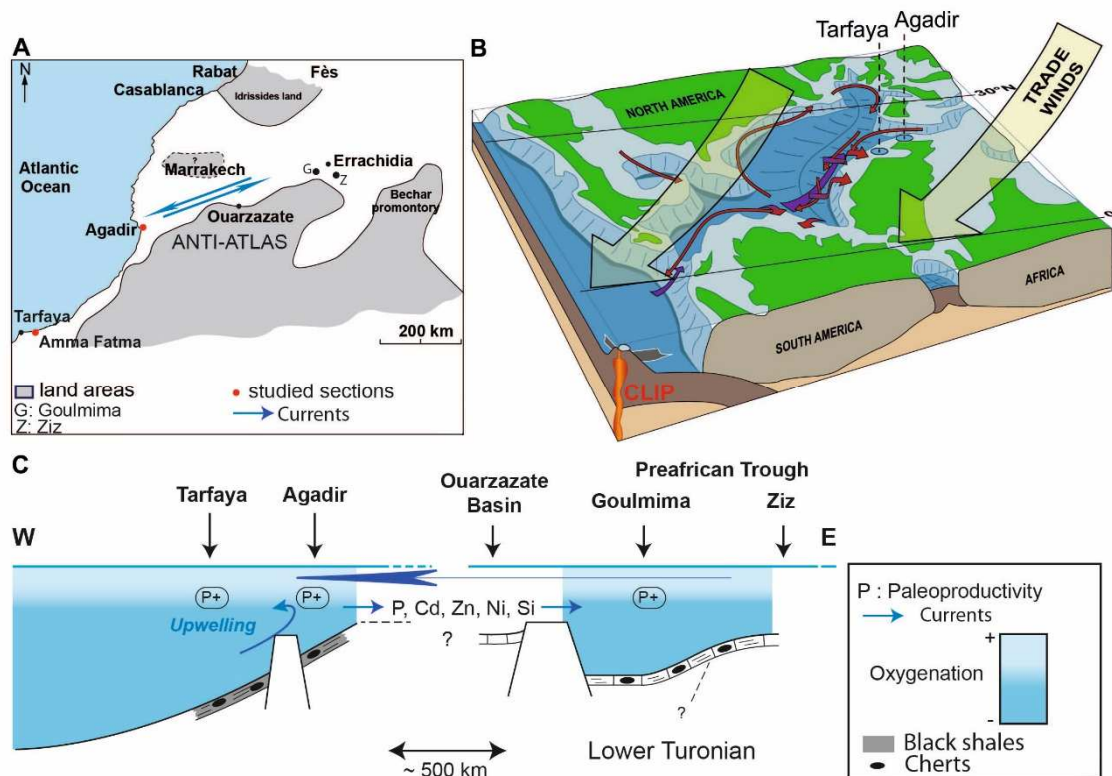
700 to be promoted by intense upwelling of nutrient-rich waters (Einsele and Wiedmann,
701 1982; Kruijs and Barron, 1990; Sinninghe Damsté and Köster, 1998; Lünig et al.,
702 2004; Kuhnt et al., 2005; Keller et al., 2008; Mort et al., 2008; Trabucho Alexandre et
703 al., 2010; Fabre et al., 2018). Foraminiferal assemblages suggest intensified upwelling
704 of relatively cool waters at Amma Fatma (Smrzka et al., 2017), while geochemical,
705 sedimentological, paleoecological and isotopic evidences at Agadir suggest intense
706 upwelling of nutrient-rich waters to explain the high marine productivity (Fabre et al.,
707 2018). According to Tyson (1993, 1995), AOM usually dominates the kerogen
708 assemblages in upwelling influenced dysoxic sediment facies, while associations with
709 high number of dinocysts, foraminiferal test-linings and fungal remains are associated
710 to upwelling areas with high oxygen availability (base of CIE at Agadir). In both basins,
711 the lower Turonian palynofacies association is dominated by AOM, with a marine
712 phytoplanktonic origin in Agadir, and dominance of bacterial material in Amma Fatma.
713 These organic facies therefore corroborate the high primary productivity previously
714 suggested for the lower Turonian of Agadir and Amma Fatma (Smrzka et al., 2017;
715 Fabre et al., 2018).

716

717 *5.4. Organic matter assemblage vs paleogeographical context*

718 In accordance to previous studies, organic petrographic and geochemical data indicate
719 oxic to temporarily dysoxic conditions during the OAE2 at Agadir, with anoxic marine
720 conditions being only established during the lower Turonian. This study therefore
721 corroborates a delay of the anoxia in shallow marginal environments like Agadir
722 (Leckie et al., 1998; Gertsh et al., 2010; Lézin et al., 2012; Lebedel et al., 2013, 2015),
723 when compared to outer shelf and deeper basin environments, like the Tarfaya Basin,
724 where the highest TOC values are normally associated to the CIE (e.g. El Albani et al.,
725 1999a; Kuypers et al., 2004a; Kolonic et al., 2005; Mort et al., 2008; Sinninghe Damsté
726 et al., 2008; Gertsh et al., 2010; Ghassal et al., 2016). Furthermore, differences in terms
727 of the redox conditions in the water column during the lower Turonian of Agadir and
728 Amma Fatma are highlighted. Agadir is characterized by dysoxic to anoxic conditions,
729 while in Amma Fatma was observed that the late Cenomanian euxinic conditions (with
730 punctual dysoxia) continue into the lower Turonian (*H. helvetica* biozone). This
731 difference could be related to the mixing of Tethyan and Atlantic waters in Agadir (Fig.
732 10, A, B), suggested by the occurrence of both Tethyan and Atlantic ammonites
733 (*Vascoceras* and *Selwynoceras*, respectively – Wiedmann et al., 1974, 1978) and

734 ostracods (Andreu, 1991). This water circulation patterns have already been proposed
 735 by Fabre et al. (2018), who suggest a connection between the Agadir Basin and the
 736 Tethyan Ocean via the Preafrican Trough (Fig. 10, C). This is not observed at Tarfaya,
 737 displaying only an Atlantic influence (Boreal fauna of North America and Northern
 738 Europe; Wiedmann et al., 1974, 1978). This leads to the conclusion that, although the
 739 Cenomanian—Turonian boundary is a period with likely black shale occurrences
 740 worldwide, local control mechanisms are also important players in the shaping of the
 741 effects of the global event in the sedimentary record.
 742



743
 744 Fig. 10. A: NW African margin paleogeographical map during the Cenomanian—
 745 Turonian (modified after Essafraoui et al. 2015; Fabre et al., 2018) with location of the
 746 two studied basins and the presumed Atlantic/Tethys connection. B: Mid-Cretaceous
 747 North Atlantic oceanographic processes. Red and purple arrows indicate surface and
 748 deep circulation, respectively (modified after Trabucho Alexandre et al. 2010; Fabre et
 749 al., 2018). C: Northwest Saharan margin oxygenation conditions and main currents
 750 during the early Turonian (modified after Fabre et al, 2018). CLIP: Caribbean Large
 751 Igneous Province. For location of Mohammed Beach section and S4, S57 and S75
 752 boreholes please see figure 1.
 753

754 **6. Conclusions**

755 The present study offers a contribution to the knowledge of the organic fraction of the
756 Cenomanian—Turonian record of the Moroccan Atlantic coast. The organic facies
757 variability allowed the definition of the paleoenvironmental conditions at time of
758 deposition of the upper Cenomanian—lower Turonian sediments of the Agadir section
759 (Agadir Basin) and of the lower Turonian record of the Amma Fatma section (Tarfaya
760 Basin).

761 The Agadir section represents a transgressive-regressive cycle during the upper
762 Cenomanian, followed by a drowning event, during the lower Turonian, with
763 establishment of a deep platform environment. Two periods of low OM preservation, at
764 the base of the section and at the base of the lower Turonian mark sea-level lowstands,
765 with a high energy oxic environment ($EFMn > 1$), that culminate in two emersion
766 surfaces. The Amma Fatma section is characterized by an organic facies dominated by
767 bacterial material, indicating a shallow water environment, with some degree of
768 restriction, euxinic conditions (high $EFMo$) and high paleoproductivity ($EFCu$, $EFNi$
769 and $EFZn > 1$).

770 The lower Turonian sediments in both sections represent environments with low oxygen
771 availability and high primary productivity, possibly promoted by the occurrence of
772 upwelling currents. Nevertheless, differences in redox conditions between Agadir and
773 Tarfaya are clear with anoxia prevailing at Agadir, while euxinic conditions are
774 established at Tarfaya. This study further corroborates a delay in the anoxia in Agadir,
775 that during the CIE only reaches slight dysoxia, and the maintenance of reducing
776 conditions in Tarfaya after the CIE.

777

778 **Acknowledgements**

779 The authors thank the team from the Laboratory of Palynofacies and Organic Facies of
780 the Federal University of Rio de Janeiro (LAFO-UFRJ) for their technical support in
781 sample preparation and all organic geochemical analyses, and Dr. Paula Alexandra
782 Gonçalves and the Laboratory of Organic Petrography of the ICT – Instituto de Ciências
783 da Terra and the Department of Geosciences, Environment and Spatial Planning of the
784 University of Porto for the photomicrographs of the whole-rock polished blocks. The
785 authors also acknowledge the MAREFOZ Laboratory, in particular Dr. Ana Cristina
786 Rocha, for technical support with $\delta^{13}C_{Kerogen}$ analysis.

787

788 **References**

- 789 Algeo, T.J., Maynard, J.B., 2004. Trace-element behavior and redox facies in core
790 shales of Upper Pennsylvanian Kansas-type cyclothems. *Chemical Geology* 206, 289–
791 318. <https://doi.org/10.1016/j.chemgeo.2003.12.009>.
- 792 Algeo, T.J., Tribovillard, N., 2009. Environmental Analysis of Paleoceanographic
793 Systems Based on Molybdenum-Uranium Covariation. *Chemical Geology* 268, 211–
794 225. <https://doi.org/10.1016/j.chemgeo.2009.09.001>.
- 795 Andreu, B., 1991. Les Ostracodes du Crétacé moyen (Barrémien à Turonien) le long
796 d'une transversale Agadir-Nador (Maroc) – Thèse: Sciences: Toulouse, Université Paul
797 Sabatier – Actes du Labo. De Géol. Sédimen. et Pal. de l'Univ. Paul Sabatier, Série 2,
798 14, 765 pp.
- 799 Arthur, M.A., Dean, W.E., Pratt, L.M., 1988. Geochemical and climatic effects of
800 increased marine organic-carbon burial at the Cenomanian-Turonian boundary. *Nature*
801 335, 714-717.
- 802 Arthur, M.A., Sageman, B.B., 1994. Marine black shales: depositional mechanisms and
803 environments of ancient deposits. *Annual Review of Earth and Planetary Sciences* 22,
804 499–551. <https://doi.org/10.1146/annurev.ea.22.050194.002435>.
- 805 ASTM Standard D4239-08, 2008. Standard Test Methods for Sulfur in the Analysis
806 Sample of Coal and Coke Using High-Temperature Tube Furnace Combustion
807 Methods. ASTM International, West Conshohocken, PA.
808 <http://dx.doi.org/10.1520/D4239-12>.
- 809 Barclay, R.S., McElwain, J.C., Sageman, B.B., 2010. Carbon sequestration activated by
810 a volcanic CO₂ pulse during Oceanic Anoxic Event 2. *Nature Geoscience* 3, 205-208.
811 <http://dx.doi.org/10.1038/NGEO757>.
- 812 Bertagnolli, A.D., Treusch, A.H., Mason, O.U., Stingl, U., Vergin, K.L., Chan, F.,
813 Beszteri, B., Giovannoni, S.J., 2011. Bacterial diversity in the bottom boundary layer of
814 the inner continental shelf of Oregon, USA. *Aquatic Microbial Ecology* 64, 15-25.
815 <http://dx.doi.org/10.3354/ame01504>.
- 816 Brumsack, H.J., 2006. The trace metal content of recent organic carbon-rich sediments:
817 Implications for Cretaceous black shale formation. *Palaeogeography,*
818 *Palaeoclimatology, Palaeoecology* 232 (2-4), 344-361.
819 <https://doi.org/10.1016/j.palaeo.2005.05.011>.
- 820 Calvert, S.E., Pedersen, T.F., 1993. Geochemistry of Recent oxic and anoxic marine
821 sediments: Implications for the geological record. *Marine Geology* 113, 67-88.
822 [https://doi.org/10.1016/0025-3227\(93\)90150-T](https://doi.org/10.1016/0025-3227(93)90150-T).
- 823 Canfield, D.E., 1994. Factors influencing organic carbon preservation in marine
824 sediments. *Chemical Geology* 114, 315–329. [https://doi.org/10.1016/0009-2541\(94\)90061-2](https://doi.org/10.1016/0009-2541(94)90061-2).

- 826 Carvalho, W.F., Rodriguez, E.G., 2004. Development of primary and bacterial
827 productivity in upwelling waters of Arraial do Cabo region, RJ (Brazil). *Brazilian*
828 *Journal of Oceanography* 52 (1), 35-45. [http://dx.doi.org/10.1590/S1679-](http://dx.doi.org/10.1590/S1679-87592004000100004)
829 87592004000100004.
- 830 Clarke, L.J., Jenkyns, H.C., 1999. New oxygen isotope evidence for long-term
831 Cretaceous climatic change in the Southern Hemisphere. *Geology* 27, 699-702.
- 832 Courtillot, V.E., Renne, P.R., 2003. On the ages of flood basalt events. *Comptes Rendus*
833 *Geoscience* 335, 113-140. [https://doi.org/10.1016/S1631-0713\(03\)00006-3](https://doi.org/10.1016/S1631-0713(03)00006-3).
- 834 Dickson, A.J., Jenkyns, H.C., Porcelli, D., van der Boorn, S., Idiz, E., 2016. Basin-scale
835 control on the molybdenum-isotope composition of seawater during Oceanic Anoxic
836 Event 2 (Late Cretaceous). *Geochimica et Cosmochimica Acta* 178, 291-306.
837 <https://doi.org/10.1016/j.gca.2015.12.036>.
- 838 Einsele, G., Wiedmann, J., 1982. Turonian black shales in the Moroccan coastal basins:
839 first upwelling in the Atlantic Ocean?, in: von Rad, U., Hinz, K., Sarnthein, M., Seibold,
840 E. (Eds.), *Geology of the Northwest African Continental Margin*. Springer, Berlin, pp.
841 396-414.
- 842 El Albani, A., Kuhnt, W., Luderer, F., Herbin, J.P., Caron, M., 1999a.
843 Palaeoenvironmental evolution of the Late Cretaceous sequence in the Tarfaya Basin
844 (Southwest of Morocco), in: Cameron, N.R., Bate, R.H., Clure, V.S. (Eds.), *The Oil and*
845 *Gas Habitats of the South Atlantic*. Geological Society, London, Special Publications,
846 153, pp. 223-240.
- 847 El Albani, A., Vachard, D., Kuhnt, W., Chellai, H., 1999b. Signature of hydrodynamic
848 activity caused by rapid sea level changes in pelagic organic-rich sediments, Tarfaya
849 Basin (southern Morocco). *Comptes Rendus de l'Académie des Sciences - Series IIA -*
850 *Earth and Planetary Science* 329, 397-404. [https://doi.org/10.1016/S1251-](https://doi.org/10.1016/S1251-8050(00)80063-4)
851 8050(00)80063-4.
- 852 El Albani, A., Vachard, D., Kuhnt, W., Thurrows, J., 2001. The role of diagenetic
853 carbonate concretions in the preservation of the original sedimentary record.
854 *Sedimentology* 48, 875-886. <https://doi.org/10.1046/j.1365-3091.2001.00398.x>.
- 855 Erba, E., Tremolada, F., 2004. Nannofossil carbonate fluxes during the Early
856 Cretaceous: phytoplankton response to nutrification episodes, atmospheric CO₂, and
857 anoxia. *Paleoceanography* 19, PA 1008. <https://doi.org/10.1029/2003PA000884>.
- 858 Erbacher, J., Friedrich, O., Wilson, P.A., Birch, H., Mutterlose, J., 2005. Stable organic
859 carbon isotope stratigraphy across Oceanic Anoxic Event 2 of Demerara Rise, western
860 tropical Atlantic. *Geochemistry, Geophysics, Geosystems* 6, Q06010,
861 <https://doi.org/10.1029/2004GC000850>.
- 862 Erbacher, J., Thurow, J., Littke, R., 1996. Evolution patterns of radiolaria and organic
863 matter variations: a new approach to identify sea-level changes in mid-Cretaceous
864 pelagic environments. *Geology* 24, 499-502.

- 865 Essafraoui, B., Ferry, S., Groshény, D., Içame, N., El Aouli, H., Masrour, M., Bulot,
866 L.G., Géraud, Y., Aoutem, M., 2015. Sequence stratigraphic architecture of marine to
867 fluvial deposits across a passive margin (Cenomanian, Atlantic margin, Morocco,
868 Agadir transect). *Carnets de Géologie* 15(12), 137-172.
- 869 Ettachfini, M., Andreu, B., 2004. Le Cénomanien et le Turonien de la Plate-forme
870 Préafricaine du Maroc. *Cretaceous Research* 25, 277-302.
871 <https://doi.org/10.1016/j.cretres.2004.01.0>.
- 872 Fabre, S., Lézin, C., Lebedel, V., 2018. Paleooceanographic significance of cerium
873 anomalies during the OAE2 on the NW African margin. *Journal of Sedimentary*
874 *Research* 88, 1284-1299. <https://doi.org/10.2110/jsr.2018.66>.
- 875 Flores, D., Suárez-Ruiz, I., 2017. Organic Petrology in the Study of Dispersed Organic
876 Matter, Chapter 2, in: Suárez-Ruiz, I., Mendonça Filho, J.G. (Eds.), *Geology: Current*
877 *and Future Developments. The Role of Organic Petrology in the Exploration of*
878 *Conventional and Unconventional Hydrocarbon Systems*. Bentham Science Publishers,
879 United Arab Emirates, vol. 1, pp. 34-76.
- 880 Forster, A., Schouten, S., Moriya, K., Wilson, P.A., Sinninghe Damsté, J.S., 2007.
881 Tropical warming and intermittent cooling during the Cenomanian/Turonian oceanic
882 anoxic event 2: sea surface temperature records from the equatorial Atlantic.
883 *Paleoceanography* 22, PA1219. <http://dx.doi.org/10.1029/2006PA001349>.
- 884 Friedrich, O., Norris, R.D., Erbacher, J., 2012. Evolution of middle to Late Cretaceous
885 oceans – a 55 my record of Earth’s temperature and carbon cycle. *Geology* 40, 107-110.
886 <http://dx.doi.org/10.1130/G32701.1>.
- 887 Gale, A.S., Hardenbol, J., Hathway, B., Kennedy, W.J., Young, J.R., Phansalkar, V.,
888 2002. Global correlation of Cenomanian (Upper Cretaceous) sequences: evidence for
889 Milankovitch control on sea level. *Geology* 30, 291-294. [https://doi.org/10.1130/0091-7613\(2002\)030<0291:GCOCUC>2.0.CO;2](https://doi.org/10.1130/0091-7613(2002)030<0291:GCOCUC>2.0.CO;2).
- 891 Gale, A.S., Voigt, S., Sageman, B.B., Kennedy, W.J., 2008. Eustatic sea-level record
892 for the Cenomanian (Late Cretaceous) – extension to the Western Interior Basin, USA.
893 *Geology* 36, 859-862. <https://doi.org/10.1130/G24838A.1>.
- 894 Ghassal, B.I., Littke, R., Sachse, V., Sindern, S., Schwarzbauer, J., 2016. Depositional
895 environment and source rock potential of Cenomanian and Turonian sedimentary rocks
896 of the Tarfaya Basin, sedimentary rocks of the Tarfaya Basin, Southwest Morocco.
897 *Geologica Acta* 14 (4), 419-441. <https://doi.org/10.1344/GeologicaActa2016.14.4.6>.
- 898 Gebhardt, H., Kuhnt, W., Holbourn, A., 2004. Foraminiferal response to sea level
899 change, organic flux and oxygen deficiency in the Cenomanian of the Tarfaya Basin,
900 southern Morocco. *Marine Micropaleontology* 53, 133-157.
901 <https://doi.org/10.1016/j.marmicro.2004.05.007>.
- 902 Gertsch, B., Adatte, T., Keller, G., Tantawy, A.A.A.M., Berner, Z., Mort, H.,
903 Fleitmann, D., 2010. Middle and late Cenomanian oceanic anoxic events in shallow and

904 deeper shelf environments of western Morocco. *Sedimentology* 57, 1430-1462.
905 <https://doi.org/10.1111/j.1365-3091.2010.01151.x>.

906 Glikson, M., Taylor, G.H., 1986. Cyanobacterial mats: major contributors to the organic
907 matter in Toolebuc Formation oil shales, in: Gravestock, D.I., Moore, P.S., Pitt, G.M.
908 (Eds.), *Contributions to the Geology and Hydrocarbon Potential of the Eromanga Basin*.
909 Geological Society of Australia, Special Publication 12, pp. 273-286.

910 Haq, B.U., 2014. Cretaceous eustasy revisited. *Global and Planetary Change* 113, 44-
911 58. <https://doi.org/10.1016/j.gloplacha.2013.12.007>.

912 Hart, M.B., Leary, P.N., 1989. The stratigraphic and paleogeographic setting of the late
913 Cenomanian anoxic event. *Journal of the Geological Society* 146, 305–310.
914 <https://doi.org/10.1144/gsjgs.146.2.0305>.

915 Huber, B.T., Hodell, D.A., Hamilton, C.P., 1995. Middle-Late Cretaceous climate of the
916 southern high latitudes: stable isotopic evidence for minimal equator-to-pole thermal
917 gradients. *GSA Bulletin* 107, 1164-1191.

918 Huber, B.T., Norris, R.D., MacLeod, K.G., 2002. Deep-sea paleotemperature record of
919 extreme warmth during the Cretaceous. *Geology* 30, 123-126.

920 ISO 7404-2, 2009. Methods for the petrographic analysis of coals — Part 2: methods of
921 preparing coal samples. International Organization for Standardization, 12 pp.

922 Jati, M., Grosheny, D., Ferry, S., Masrour, M., Aoutem, M., Içame, N., Gauthier-
923 Lafaye, F., Desmares, D., 2010. The Cenomanian-Turonian boundary event on the
924 Moroccan Atlantic margin (Agadir basin): Stable isotope and sequence stratigraphy.
925 *Palaeogeography, Palaeoclimatology, Palaeoecology* 296, 151-164.
926 <https://doi.org/10.1016/j.palaeo.2010.07.002>

927 Jenkyns, H.C., 1980. Cretaceous anoxic events – from continents to oceans. *Journal of*
928 *the Geological Society* 137, 171-188.

929 Jenkyns, H.C., 2010. Geochemistry of oceanic anoxic events. *Geochemistry,*
930 *Geophysics, Geosystems* 11, Q03004. <http://dx.doi.org/10.1029/2009GC002788>.

931 Keller, G., Adatte, T., Berner, Z., Chellai, E.H., Stueben, D., 2008. Oceanic events and
932 biotic effects of the Cenomanian-Turonian anoxic event, Tarfaya Basin, Morocco.
933 *Cretaceous Research* 29, 976-994. <https://doi.org/10.1016/j.cretres.2008.05.020>.

934 Keller, G., Berner, Z., Adatte, T., Stueben, D., 2004. Cenomanian–Turonian and delta
935 C-13, and delta O-18, sea level and salinity variations at Pueblo, Colorado.
936 *Palaeogeography, Palaeoclimatology, Palaeoecology* 211, 19–43.

937 Keller, G., Han, Q., Adatte, T., Burns, S.J., 2001. Palaeoenvironment of the
938 Cenomanian–Turonian transition at Eastbourne, England. *Cretaceous Research* 22, 391–
939 422.

940 Keller, G., Pardo, A., 2004. Age and paleoenvironment of the Cenomanian–Turonian
941 global stratotype section and point at Pueblo, Colorado. *Marine Micropaleontology* 51,
942 95–128.

943 Kerr, A.C., 1998. Oceanic plateau formation: a cause of mass extinction and black shale
944 deposition around the Cenomanian-Turonian boundary? *Journal of the Geological*
945 *Society London* 155, 619-626.

946 Kolonic, S., Sinninghe Damsté, J.S., Böttcher, M.E., Kuypers, M.M.M., Kuhnt, W.,
947 Beckmann, B., Scheeder, G., Wagner, T., 2002. Geochemical characterization of
948 Cenomanian/Turonian black shales from the Tarfaya Basin (SW Morocco). *Journal of*
949 *Petroleum Geology* 25 (3), 325-350. [https://doi.org/10.1111/j.1747-](https://doi.org/10.1111/j.1747-5457.2002.tb00012.x)
950 [5457.2002.tb00012.x](https://doi.org/10.1111/j.1747-5457.2002.tb00012.x).

951 Kolonic, S., Wagner, T., Forster, A., Sinninghe Damsté, J.S., Walsworth-Bell, B., Erba,
952 E., Turgeon, S., Brumsack, H.J., Chellai, E.H., Tsikos, H., Kuhnt, W., Kuypers,
953 M.M.M., 2005. Black shale deposition on the northwest African shelf during the
954 Cenomanian-Turonian oceanic anoxic event: climate coupling and global organic
955 carbon burial. *Paleoceanography* 20, PA1006.

956 Krujic, E., Barron, E., 1990. Climate model prediction of paleoproductivity and
957 potential source-rock distribution, in: Huc, A.Y. (Ed.), *Deposition of Organic Facies*.
958 American Association of Petroleum Geologists, *Studies in Geology* 94, pp. 147-159.

959 Kuhnt, W., El Chellai, H., Holbourn, A., Luderer, F., Thirrow, J., Wagner, T., El
960 Albani, A., Beckmann, B., Herbin, J.P., Kawamura, H., Kolonic, S., Nederbragt, S.,
961 Street, C., Ravillious, K., 2001. Morocco Basin's sedimentary records may provide
962 correlations for Cretaceous paleoceanographic events worldwide. *Eos, Transactions*
963 *American Geophysical Union* 82 (33), 361-364. <https://doi.org/10.1029/01EO00223>.

964 Kuhnt, W., Holbourn, A.E., Beil, S., Aquit, M., Krawczyk, T., Flögel, S., Chellai, E.H.,
965 Jabour, H., 2017. Unraveling the onset of Cretaceous Oceanic Anoxic Event 2 in an
966 extended sediment archive from the Tarfaya-Laayoune Basin, Morocco.
967 *Paleoceanography* 32, 923-946. <https://doi.org/10.1002/2017PA003146>.

968 Kuhnt, W., Holbourn, A., Gale, A., Chellai, E.H., Kennedy, W.J., 2009. Cenomanian
969 sequence stratigraphy and sea-level fluctuations in the Tarfaya Basin (SW Morocco).
970 *GSA Bulletin* 121, 1695-1710. <https://doi.org/10.1130/B26418.1>.

971 Kuhnt, W., Luderer, F., Nederbragt, S., Thirrow, J., Wagner, T., 2005. Orbital-scale
972 record of the late Cenomanian-Turonian oceanic anoxic event (OAE-2) in the Tarfaya
973 Basin (Morocco). *International Journal of Earth Sciences* 94, 147-159.

974 Kuhnt, W., Nederbragt, A., Leine, L., 1997. Cyclicity of Cenomanian-Turonian
975 organic-carbon-rich sediments in the Tarfaya Atlantic Coastal Basin (Morocco).
976 *Cretaceous Research* 18, 587-601. <https://doi.org/10.1006/crel.1997.0076>.

977 Kuhnt, W., Wiedmann, J., 1995. Cenomanian-Turonian source rocks:
978 paleobiogeographic and paleoenvironmental aspects, in: Huc, A.Y. (Ed.),
979 *Paleogeography, Paleoclimate and Source Rocks*. AAPG *Studies in Geology* 40, Tulsa,
980 OK, pp. 213-232.

981 Kuypers, M.M.M., Lourens, L.J., Rijpstra, W.I.C., Pancost, R.D., Nijenhuis, I.A.,
982 Sinninghe Damsté, J.S.S., 2004a. Orbital forcing of organic carbon burial in the proto-

983 North Atlantic during oceanic anoxic event 2. *Earth and Planetary Science Letters* 228,
984 465–482. <https://doi.org/10.1016/j.epsl.2004.09.037>.

985 Kuypers, M.M.M., van Breugel, Y., Schouten, S., Erba, E., Sinninghe Damsté, J.S.,
986 2004b. N₂-fixing cyanobacteria supplied nutrient N for Cretaceous oceanic anoxic
987 events. *Geology* 32(10), 853-856.

988 Larson, R.L., 1991. Latest pulse of earth-evidence for a mid-Cretaceous superplume.
989 *Geology* 19, 547-550.

990 Larson, R.L., Erba, E., 1999. Onset of the mid-Cretaceous greenhouse in the Barremian-
991 Aptian: igneous events and the biological, sedimentary, and geochemical responses.
992 *Paleoceanography* 14, 663-678.

993 Lavik, G., Stührmann, T., Brüchert, V., Van der Plas, A., Mohrholz, V., Lam, P.,
994 Mußmann, M., Fuchs, B.M., Amann, R., Lass, U., Kuypers, M.M.M., 2008.
995 Detoxification of sulphidic African shelf waters by blooming chemolithotrophs. *Nature*
996 457, 581-584. <https://doi.org/10.1038/nature07588>.

997 Lebedel, V., 2013. Enregistrement de l'évènement anoxique Cénomaniensupérieur-
998 Turonien inférieur à l'ouest de la plateforme saharienne : sédimentologie, paléontologie,
999 géochimie et minéralogie. PhD. thesis, Université de Toulouse, Toulouse, France, 294
1000 pp.

1001 Lebedel, V., Lézin, C., Andreu, B., Ettachfini, E.M., Grosheny, D., 2015. The upper
1002 Cenomanian-lower Turonian of the Preafrican Trough (Morocco): Platform
1003 configuration and palaeoenvironmental conditions. *Journal of African Earth Sciences*
1004 106, 1-16. <http://dx.doi.org/10.1016/j.jafrearsci.2015.03.001>.

1005 Lebedel, V., Lézin, C., Andreu, B., Wallez, M.-J., Ettachfini, E.M., Riquier, L., 2013.
1006 Geochemical and palaeoecological record of the Cenomanian-Turonian Anoxic Event in
1007 the carbonate platform of the Preafrican Trough, Morocco. *Palaeogeography,*
1008 *Palaeoclimatology, Palaeoecology* 369, 79-98.
1009 <http://dx.doi.org/10.1016/j.palaeo.2012.10.005>.

1010 Leckie, E.M., Bralower, T.J., Cashman, R., 2002. Oceanic anoxic events and plankton
1011 evolution: biotic response to tectonic forcing during the mid-Cretaceous.
1012 *Paleoceanography* 17, 13.1-13.29.

1013 Leckie, R.M., Yurevitch, R.M., West, O.L., Finkelstein, D., Schmid, M.G., 1998.
1014 Paleoceanography of the southwestern Western Interior sea during the time of the
1015 Cenomanian–Turonian boundary (Late Cretaceous), in: Dean, W.E., Arthur, M.A.
1016 (Eds.), *Stratigraphy and Paleoenvironments of the Cretaceous Interior Seaway*. SEPM
1017 *Concepts in Sedimentology and Paleontology* 6, USA, pp. 101–126.

1018 Lenniger, M., Nøhr-Hansen, H., Hills, L.V., Bjerrum, C.J., 2014. Artic black-shale
1019 formation during Cretaceous Oceanic Anoxic Event 2. *Geology* 42 (9), 799-802.
1020 <https://doi.org/10.1130/G35732.1>.

- 1021 Lézin, C., Andreu, B., Ettachfani, E.M., Wallez, M.-J., Lebedel, V., Meister, C., 2012.
1022 The Upper Cenomanian-Lower Turonian of the Preafrican Trough, Morocco.
1023 *Sedimentary Geology* 245-246, 1-16. <https://doi.org/10.1016/j.sedgeo.2011.12.003>.
- 1024 Lüning, S., Kolonic, S., Belhadj, E.M., Belhadj, Z., Cota, L., Baríc, G., Wagner, T.,
1025 2004. Integrated depositional model for the Cenomanian-Turonian organic-rich strata in
1026 North Africa. *Earth-Science Reviews* 64, 51-117. [https://doi.org/10.1016/S0012-](https://doi.org/10.1016/S0012-8252(03)00039-4)
1027 [8252\(03\)00039-4](https://doi.org/10.1016/S0012-8252(03)00039-4).
- 1028 Madigan, M.T., Martinko, J.M., Bender, K.S., Buckley, D.H., Stahl, D.A., 2015. Brock
1029 *Biology of Microorganisms* (Fourteenth edition.). Pearson, Boston.
- 1030 Manske, A.K., Glaeser, J., Kuypers, M.M.M., Overmann, J., 2005. Physiology and
1031 Phylogeny of Green Sulfur Bacteria Forming a Monospecific Phototropic Assemblage
1032 at a Depth of 100 Meters in the Black Sea. *Applied and Environmental Microbiology*
1033 71(12), 8049-8060. <https://doi.org/10.1128/AEM.71.12.8049-8060.2005>.
- 1034 Marschall, E., Jogler, M., Henßge, U., Overmann, J., 2010. Large-scale distribution and
1035 activity patterns of an extremely low-light-adapted population of green sulfur bacteria in
1036 the Black Sea. *Environmental Microbiology* 12(5), 1348-1362.
1037 <https://doi.org/10.1111/j.1462-2920.2010.02178.x>.
- 1038 Mendonça Filho, J.G., Gonçalves, P.A., 2017. Organic Matter: Concepts and
1039 Definitions, Chapter 1, in: Suárez-Ruiz, I., Mendonça Filho, J.G. (Eds.), *Geology:*
1040 *Current and Future Developments. The Role of Organic Petrology in the Exploration of*
1041 *Conventional and Unconventional Hydrocarbon Systems*. Bentham Science Publishers,
1042 United Arab Emirates, vol. 1, pp. 1-33.
- 1043 Mendonça Filho, J.G., Chagas, R.B.A., Menezes, T.R., Mendonça, J.O., da Silva, F.S.,
1044 Sabadini-Santos, E., 2010a. Organic facies of the Oligocene lacustrine system in the
1045 Cenozoic Taubaté basin, Southern Brazil. *International Journal of Coal Geology* 84,
1046 <https://doi.org/10.1016/j.coal.2010.07.004>.
- 1047 Mendonça Filho, J.G., Menezes, T.R., Mendonça, J.O., Oliveira, A.D., Carvalho, M.A.,
1048 Sant'Anna, A.J.; Souza, J.T., 2010b. Palinofácies, in: Carvalho, I.S. (Ed.),
1049 *Paleontologia*, Rio de Janeiro, Interciência 2, pp. 379-413.
- 1050 Mendonça Filho, J.G., Menezes, T.R., Mendonça, J.O., Oliveira, A.D., Silva, T.F.,
1051 Rondon, N.F., Silva, F.S., 2012. Organic facies: Palynofacies and organic geochemistry
1052 approaches, in: Panagiotaras, D. (Ed.), *Geochemistry - Earth's system processes*.
1053 InTech, Rijeka, pp 211–248. <http://dx.doi.org/10.5772/47928>.
- 1054 Mendonça Filho, J.G., Menezes, T.R., Mendonça, J.O., 2014a. Organic Composition
1055 (Palynofacies Analysis). 7th ICCP Training Course on Dispersed Organic Matter, GFZ
1056 (Deutsches GeoForschungsZentrum), Potsdam, Germany. 2014, Chapter 5, 36-89.
- 1057 Mendonça Filho, J.G., Menezes, T.R., Mendonça, J.O., Oliveira, A.D., 2014b. Kerogen:
1058 Composition and Classification. 7th ICCP Training Course on Dispersed Organic
1059 Matter, GFZ (Deutsches GeoForschungsZentrum), Potsdam, Germany. 2014, Chapter 3,
1060 17-24.

1061 Mendonça Filho, J.G., Oliveira, A.D., Souza, J.T., Mendonça, J.O., Flores, D., 2016.
1062 The fossil record of hydrozoans in dispersed organic matter: a palynofacies and organic
1063 petrographic approach to kerogen characterization, in: Demchuk, T., O’Keefe, J.,
1064 Gentzis, T., Curiale, J. (Eds.), *TSOP The Society for Organic Petrology – ICCP*
1065 *International Committee for Coal and Organic Petrology – AASP The Palynological*
1066 *Society 2016 Joint Meeting Abstract Book*, Houston, Texas, USA, pp. 84-86. Published
1067 as a supplement to *AASP-The Palynological Society Newsletter* 49-3, ISSN 0732-6041.

1068 Mort, H.P., Adatte, T., Foellmi, K.B., Keller, G., Steinmann, P., Matera, V., Berner, Z.,
1069 Stueben, D., 2007. Phosphorus and the roles of productivity and nutrient recycling
1070 during Oceanic Event 2. *Geology* 35, 483–486. <https://doi.org/10.1130/G23475A.1>.

1071 Mort, H.P., Adatte, T., Keller, G., Bartels, D., Follmi, K.B., Steinmann, P., Berner, Z.,
1072 Chellai, E.H., 2008. Organic carbon deposition and phosphorus accumulation during
1073 Oceanic Anoxic Event 2 in Tarfaya, Morocco. *Cretaceous Research* 29, 1009-1023.
1074 <https://doi.org/10.1016/j.cretres.2008.05.026>.

1075 Norris, R.D., Bice, K.L., Magno, E.A., Wilson, P.A., 2002. Jiggling the tropical
1076 thermostat in the Cretaceous hothouse. *Geology* 30, 299-302.

1077 Nzoussi-Mbassani, P., Khamli, N., Disnar, J.R., Laggoun-Défarge, F., Boussafir, M.,
1078 2005. Cenomanian-Turonian organic sedimentation in North-West Africa: A
1079 comparison between the Tarfaya (Morocco) and Senegal Basins. *Sedimentary Geology*
1080 177, 271-295. <https://doi.org/10.1016/j.sedgeo.2005.03.008>.

1081 O’Brien, C.L., Robinson, S.A., Pancost, R.D., Damsté, J.S.S., Schouten, S., Lunt, D.J.,
1082 Alsenz, H., Bornemann, A., Bottini, C., Brassel, S.C., Farnsworth, A., Forster, A.,
1083 Huber, B.T., Inglis, G.N., Jenkyns, H.C., Linnert, C., Littler, K., Markwick, P.,
1084 McAnena, A., Mutterlose, J., Naafs, B.D.A., Püttmann, W., Sluijs, A., van Helmond,
1085 N.A.G.M., Vellekoop, J., Wagner, T., Wrobel, NE., 2017. Cretaceous sea-surface
1086 temperature evolution: constraints from TEX86 and planktonic foraminiferal oxygen
1087 isotopes. *Earth-Science Reviews* 172, 224-247.
1088 <http://dx.doi.org/10.1016/j.earscirev.2017.07.012>.

1089 O’Connor, L.K., Robinson, S.A., Naafs, B.D., Jenkyns, H.C., Henson, S., Clarke, M.,
1090 Pancost, R.D., 2019. Late Cretaceous temperature evolution of the southern high
1091 latitudes: a TEX86 perspective. *Paleoceanography and Paleoclimatology* 34, 436-454.
1092 <https://doi.org/10.1029/2018PA003546>.

1093 Owen, J.D., Reinhard, C.T., Rohrssen, M., Love, G.D., Lyons, T.W., 2016. Empirical
1094 links between trace metal cycling and marine microbial ecology during a large
1095 perturbation to Earth’s carbon cycle. *Earth and Planetary Science Letters* 449, 407-417.
1096 <http://dx.doi.org/10.1016/j.epsl.2016.05.046>.

1097 Paul, C.R.C., Lamolda, M.A., Mitchell, S.F., Vaziri, M.R., Gorostidi, A., Marshall, J.D.,
1098 1999. The Cenomanian–Turonian boundary at Eastbourne (Sussex, UK): a proposed
1099 European reference section. *Paleogeography, Palaeoclimatology, Palaeoecology* 150,
1100 83–121.

- 1101 Pedersen, T.F., Calvert, S.E., 1990. Anoxia vs Productivity – what controls the
1102 formation of organic-carbon-rich sediments and sedimentary rocks. AAPG Bulletin 74,
1103 454–466. <https://doi.org/10.1306/0C9B232B-1710-11D7-8645000102C1865D>.
- 1104 Peters, K.E., Walters, C.C., Moldowan, J.M., 2005. The Biomarker Guide. Volume 1:
1105 Biomarkers and Isotopes in the Environment and Human History. Volume 2:
1106 Biomarkers and Isotopes in Petroleum Exploration and Earth History. 2nd Edition,
1107 Cambridge University Press, New York.
- 1108 Pickel, W., Kus, J., Flores, D., Kalaitzidis, S., Christianis, K., Cardott, B.J., Misz-
1109 Kennan, M., Rodrigues, S., Hentschel, A., Hamor-Vido, M., Crosdale, P., Wagner, N.,
1110 ICCP, 2017. Classification of liptinite – ICCP System 1994. International Journal of
1111 Coal Geology 169, 40-61. <http://dx.doi.org/10.1016/j.coal.2016.11.004>.
- 1112 Poulton, S.W., Henkel, S., März, C., Urquhart, H., Floegel, S., Kasten, S., Sinninghe
1113 Damsté, J., Wagner, T., 2015. A continental-weathering control on orbitally driven
1114 redox-nutrient cycling during Cretaceous Oceanic Anoxic Event 2. *Geology* 43 (11),
1115 963-966. <https://doi.org/10.1130/G36837.1>.
- 1116 Prauss, M.L., 2012. The Cenomanian/Turonian Boundary event (CTBE) at Tarfaya,
1117 Morocco: Palaeoecological aspects as reflected by marine palynology. *Cretaceous*
1118 *Research* 34, 233-256. <https://doi.org/10.1016/j.cretres.2011.11.004>.
- 1119 Pucéat, E., Lécuyer, C., Sheppards, S.M.F., Dromart, G., Reboulet, S., Grandjean, P.,
1120 2003. Thermal evolution of Cretaceous Tethyan marine waters inferred from oxygen
1121 isotope composition of fish tooth enamels. *Paleoceanography* 18, 1029.
1122 <http://dx.doi.org/10.1029/2002PA000823>.
- 1123 Raven, M.R., Fike, D.A., Bradley, A.S., Gomes, M.L., Owens, J.D., Webb, S.A., 2019.
1124 Paired organic matter and pyrite $\delta^{34}\text{S}$ records reveal mechanisms of carbon, sulfur, and
1125 iron cycle disruption during Ocean Anoxic Event 2. *Earth and Planetary Science Letters*
1126 512, 27-38. <https://doi.org/10.1016/j.epsl.2019.01.048>.
- 1127 Ricci, J.N., Coleman, M.L., Welander, P.V., Sessions, A.L., Summons, R.E., Spear,
1128 J.R., Newman, D.K., 2014. Diverse capacity for 2-methylhopanoid production
1129 correlates with a specific ecological niche. *International Society for Microbial Ecology*
1130 *Journal* 8, 675-684. <http://dx.doi.org/10.1038/ismej.2013.191>.
- 1131 Schlanger, S.O., Jenkyns, H.C., 1976. Cretaceous oceanic anoxic event: causes and
1132 consequences. *Geol. Mijnbouw* 55, 179–188.
- 1133 Sinninghe Damsté, J.S., Köster, J., 1998. A euxinic southern North Atlantic Ocean
1134 during the Cenomanian-Turonian oceanic anoxic event. *Earth and Planetary Science*
1135 *Letters*, 158, 165-173. [https://doi.org/10.1016/S0012-821X\(98\)00052-1](https://doi.org/10.1016/S0012-821X(98)00052-1).
- 1136 Sinninghe Damsté, J.S., Kuypers, M.M.M., Pancost, R.R., Schouten, S., 2008. The
1137 carbon isotopic response of algae, (cyano)bacteria, archaea and higher plants to the late
1138 Cenomanian perturbation of the global carbon cycle: Insights from biomarkers in black
1139 shales from the Cape Verde Basin (DSDP Site 367). *Organic Geochemistry* 39, 1703–
1140 1718. <https://doi.org/10.1016/j.orggeochem.2008.01.012>.

- 1141 Sinninghe Damsté, J.S., van Bentum, E.C., Reichart, G.J., Pross, J., Schouten, S., 2010.
1142 A CO₂ decrease-driven cooling and increased latitudinal temperature gradient during the
1143 mid-Cretaceous Oceanic Anoxic Event 2. *Earth Planetary Science Letters* 293, 97-103.
1144 <http://dx.doi.org/10.1016/j.epsl.2010.02.027>.
- 1145 Sinninghe Damsté, J.S., Wakeham, S.G., Kohnen, M.E.L., Hayes, J.M., de Leeuw,
1146 J.W., 1993. A 6000 year sedimentary molecular record of chemocline excursions in the
1147 Black Sea. *Nature* 362, 827-829. <https://doi.org/10.1038/362827a0>.
- 1148 Sinton, C.W., Duncan, R.A., Storey, M., Lewis, J., Estrada, J.J., 1998. An oceanic flood
1149 basalt province within the Caribbean Plate. *Earth and Planetary Science Letters* 155,
1150 221-235.
- 1151 Smrzka, D., Zwicker, J., Kolonic, S., Birgel, D., Little, C.T.S., Marzouk, A.M., Chellai,
1152 E.H., Wagner, T., Peckmann, J., 2017. Methane seepage in a Cretaceous greenhouse
1153 world recorded by an unusual carbonate deposit from the Tarfaya Basin, Morocco. *The*
1154 *Depositional Record* 3 (1), 4-37. <https://doi.org/10.1002/dep2.24>.
- 1155 Snow, L.J., Duncan, R.A., Bralower, T.J., 2005. Trace element abundances in the Rock
1156 Canyon Anticline, Pueblo, Colorado, marine sedimentary section and their relationship
1157 to Caribbean plateau construction and oxygen anoxic event 2. *Paleoceanography* 20,
1158 PA3005. <https://doi.org/10.1029/2004PA001093>.
- 1159 Stankiewicz, A.B., Kruge, A.M., Mastalerz, M., Salomon, L.G., 1996. Geochemistry of
1160 the alginite and amorphous organic matter from Type II-S kerogens. *Organic*
1161 *Geochemistry* 24, 495-509.
- 1162 Summerhayes, C.P., 1983. Sedimentation of organic matter in upwelling regimes, in:
1163 Thiede, F., Suess, E. (Eds.), *Coastal upwelling – its sediment record. Part B:*
1164 *Sedimentary Records of Ancient Coastal Upwelling*. Plenum Press, New York, 29–72.
- 1165 Summons, R.E., Jahnke, L.L., Hope, J.M., Logan, G.A., 1999. 2-Methylhopanoids as
1166 biomarkers for cyanobacterial oxygenic photosynthesis. *Nature* 400, 554-557.
- 1167 Takashima, R., Nishi, H., Huber, B., Leckie, R.M., 2006. Greenhouse world and the
1168 Mesozoic Ocean. *Oceanography* 19, 82-92. <http://dx.doi.org/10.5670/oceanog.2006.07>.
- 1169 Ten Haven, H.L., Littke, R., Rullkötter, J., Stein, R., Welte, D.H., 1990. Accumulation
1170 rates and composition of organic matter in Late Cenozoic sediments underlying the
1171 active upwelling area off Peru. *Proceedings ODP, Scientific Results* 112, 591-606.
- 1172 Trabucho Alexandre, J., Tuenter, E., Henstra, G.A., van der Zwank, K.J., van de Wal,
1173 R.S.W., Dijkstra, H.A., de Boer, P.L., 2010. The mid-Cretaceous North Atlantic
1174 nutrient trap: black shales and OAEs. *Paleoceanography* 25, PA4201.
1175 <https://doi.org/10.1029/2010PA001925>.
- 1176 Tribovillard, N., Algeo, T.J., Baudin, F., Riboulleau, A., 2012. Analysis of marine
1177 environmental conditions based on molybdenum-uranium covariation – Applications to
1178 Mesozoic paleoceanography. *Chemical Geology* 324-325, 46-58.
1179 <https://doi.org/10.1016/j.chemgeo.2011.09.009>.

- 1180 Tribovillard, N., Algeo, T.J., Lyons, T., Riboulleau, A., 2006. Trace metals as
1181 paleoredox and paleoproductivity proxies: An update. *Chemical Geology* 232, 12-32.
1182 <https://doi.org/10.1016/j.chemgeo.2006.02.012>.
- 1183 Tribovillard, N., Riboulleau, A., Lyons, T., Baudin, F., 2004. Enhanced trapping of
1184 molybdenum by sulfurized organic matter of marine origin as recorded by various
1185 Mesozoic formations. *Chemical Geology* 213, 385–401.
1186 <https://doi.org/10.1016/j.chemgeo.2004.08.011>.
- 1187 Tsikos, H., Jenkyns, H.C., Walsworth-Bell, B., Petrizzo, M.R., Forster, A., Kolonic, S.,
1188 Erba, E., Premoli Silva, I., Baas, M., Wagner, T., Sinninghe Dameste, J.S., 2004.
1189 Carbon-isotope stratigraphy recorded by the Cenomanian–Turonian Oceanic anoxic
1190 event: correlation and implications based on three key localities. *Journal of the*
1191 *Geological Society, London* 161, 711–719.
- 1192 Turgeon, S.C., Creaser, R.A., 2008. Cretaceous oceanic anoxic event 2 triggered by a
1193 massive magmatic episode. *Nature* 454, 323–326.
- 1194 Tyson, R.V., 1993. Palynofacies analysis, in: Jenkins, D.J. (Ed.), *Applied*
1195 *Micropalaeontology*, Kluwer, Dordrecht, pp. 153-191.
- 1196 Tyson, R.V., 1995. *Sedimentary Organic Matter. Organic facies and palynofacies.*
1197 Chapman and Hall, London. <http://dx.doi.org/10.1007/978-94-011-0739-6>.
- 1198 United States Environmental Protection Agency (U.S.EPA), 2002. *Methods for the*
1199 *Determination of Total Organic Carbon (TOC) in Soils and Sediments.* Ecological Risk
1200 Assessment Support Center. NCEA-C-1282. Office of Research and Development, Las
1201 Vegas.
- 1202 Van Gemerden, H., Mas, J., 1995. Ecology of phototrophic sulfur bacteria, in:
1203 Blankenship R.E., Madigan M.T., Bauer C.E. (Eds.), *Anoxygenic Photosynthetic*
1204 *Bacteria. Advances in Photosynthesis and Respiration.* Springer, Dordrecht, vol 2, pp.
1205 49-85.
- 1206 Voigt, S., Gale, A.S., Floegel, S., 2004. Midlatitude shelf seas in the Cenomanian-
1207 Turonian greenhouse world: temperature evolution and North Atlantic circulation.
1208 *Paleoceanography* 19, PA4020. <http://dx.doi.org/10.1029/2004PA001015>.
- 1209 Wedepohl, K.H., 1995. The composition of the continental crust. *Geochimica et*
1210 *Cosmochimica Acta* 59 (7), 1217-1232. [https://doi.org/10.1016/0016-7037\(95\)00038-2](https://doi.org/10.1016/0016-7037(95)00038-2).
- 1211 Wiedmann, J., Dietl, G., Einsele, G., Immel, H., 1974. Ammoniten als Milieu-
1212 Indikationen?, in: 9 Sonderheft Geowiss-Tagung, Frankfurt-am-Main, 1973, *Nachr.*
1213 *dtsh. Geol. Ges.*, pp. 135-141.
- 1214 Wiedmann, J., Einsele, G., Immel, H., 1978. Evidence faunistique et sédimentologique
1215 pour un upwelling dans le bassin côtier de Tarfaya, Maroc, dans la Crétacé supérieur.
1216 *Ann. des Mines et de la Géol. Tunis* 28 (II), 415-441.
- 1217 Wignall, P.B., 2001. Large igneous provinces and mass extinctions. *Earth-Science*
1218 *Reviews* 53, 1-33. [https://doi.org/10.1016/S0012-8252\(00\)00037-4](https://doi.org/10.1016/S0012-8252(00)00037-4).